5-8-2004

Effects of Extreme Low Temperature on Composite Materials

Sridevi Kichhannagari
University of New Orleans

EFFECTS OF EXTREME LOW TEMPERATURE ON COMPOSITE MATERIALS

A Thesis

Submitted to the Graduate Faculty of the
University of New Orleans
in partial fulfillment of the
requirements for the degree of

Masters of Science
in
The Department of Mechanical Engineering

by

Sridevi Kichhannagari
B.Tech., Jawaharlal Nehru Technological University, India, 2001
August 2004

ACKNOWLEDGEMENT

I would like to express my sincere thanks to Dr. David Hui, my major professor and advisor for this thesis, for sharing his wisdom throughout this research and my graduate career. I am grateful to Dr. Piyush K. Dutta (US Army Cold Regions Research and Engineering Laboratories, CRREL) for his technical advice and substantial support in organizing this work, throughout the critical stages of research and also for his valuable guidance and support in my personal and professional life.

I wish to thank Mr. Glenn D. Durrell (US Army, CRREL) for his technical assistance in using the material testing system machine and Dr. David M. Cole (US Army, CRREL) for his guidance in using acoustic emission equipment.

I am grateful to Dr. Melody A. Verges, Dr. Paul J. Schilling, and Dr. Carsie A. Hall members of my thesis committee for their valuable time and patience in reviewing this work.

TABLE OF CONTENTS

ABSTRACT

This thesis discusses the effect of cryogenic temperatures on composite materials. The work includes estimating the shear strength of carbon/epoxy and glass/polyester composites at low temperatures and finding the rate of generation of microcracks in composites at cryogenic temperatures by acoustic emission technique. Microcracks increase the permeability of composites. So to study the permeability growth with microcracks, equipment is also designed to measure the permeability of composite to low temperature fluids.

With short beam shear testing it was observed that the shear strength of composites increases with decreasing temperatures. Also carbon/epoxy composites were found to be much stronger than glass/polyester composites. Cryogenic temperatures improve the strength of composites but also generate microcracks in the structure due to the thermal expansion mismatch between the matrix and fiber. With acoustic emission testing from room to –150ºC, it was found that the rate of generation of microcracks increases with reducing temperatures. The work is extended to design a permeability equipment.

1. Introduction

Composites offer several advantages over conventional materials, which include improved strength, stiffness, impact resistance, thermal conductivity and corrosion resistance. A composite is a structural material, which consists of combining two or more constituents. The constituents are combined at a macroscopic level and are not soluble in each other. In polymeric composites, one constituent is the reinforcing fiber and the one in which it is embedded is the matrix.

In near future composites are being considered by NASA re-entry vehicles. The structural systems of such re-entry space vehicles include lightweight composite fuel tanks, which contain liquid oxygen and hydrogen at cryogenic temperatures. Cryogenic engineering deals with the practical application of very low temperature processes and techniques, and fiber reinforced polymeric (FRP) composites have a long history of cryogenic applications. The development of fiber composites is a great step forward in the quest for strong materials, which can sustain low temperatures. CFRP (carbon fiber reinforced polymer) and GFRP (glass fiber reinforced polymer) composites have been used since 1970s for applications in satellites and space vehicles, which require high specific strength and high specific modulus. (i.e. ratios of strength and Young's modulus to density of the material respectively).

The cryogenic vessels for space launch vehicles have been proposed to be built using CFRP composites, which must not leak excessively, even after multiple launches.

These tanks hold fluids at temperatures ranging from -325°F to -425°F. The low temperatures introduce large residual stresses in composite components because of the thermal expansion mismatch between the fibers and the resin, which produce microcracks in the composites. Also the strength has to be maintained at cryogenic temperatures. So the interest grows in studying the rate of generation of these microcracks at cryogenic temperatures and its effect on strength of composites.

The microcracks in composites may cause leakage of fuels. Permeability is a measure of how easily a given material can be penetrated by a fluid or gas. Hence the study of permeability of composites to space fuels/gases in the cryogenic temperatures is of much importance.

Problem Definition

As said earlier, the mechanical properties of a composite material such as shear strength are greatly influenced by the cryogenic temperatures and the microcracks formed at such low temperatures can cause severe degradation of mechanical properties. They may also increase the permeability. The increased permeability may result in leakage of the fuel through the composite wall of the storage vessel and can lead to unacceptable loss of fuels. Hence the development of microcracks in composites should be seriously considered in the design and fabrication of the reusable fuel vessels of space vehicles.

Objective

The objective of this research is to characterize the mechanical performance of GFRP and CFRP composites at low temperatures. Special emphasis will be given to

study the generation, detection and monitoring of microcracks growth at cryogenic temperatures. Studies will be also made of the effects of microcracks on the increase of permeability by exposure to cryogenic temperatures and designing equipment to measure the permeability of composites to cryogenic fluids.

2. Background

2.1 Use of composites in space and damage due to cryogenic temperatures

Composite materials are ideal for structural applications where high strength to weight and stiffness to weight ratios are required. Aircraft and spacecraft are typical weight sensitive structures in which composite materials are cost effective. In NASA's re-entry vehicles composites will be used for fuel tanks, which should maintain integrity at cryogenics temperatures (below -150ºC). Work done by various authors related to this field is summarized in this chapter.

According to Cogswell (1992) space environments contain five factors not usually encountered elsewhere: intense radiation, extreme temperature excursions, vacuum atomic oxygen and the potential for high velocity impact from micrometeorites. Combination of environments poses particular problems. Radiation attack may degrade the matrix. Vacuum may cause such volatiles to be evolved and condense on sensitive instruments. If degraded products were tapped with in the matrix, they would alter mechanical performance, potentially plasticizing the composite at high temperature and embrittling it at low temperature.

According to Michelove (1979) the question of cryogenic survival is the most germane, since the others need not be considered if the material cannot withstand exposure to temperatures below 150K, the arbitrary upper limit for composites technology.

Dutta and Lord (1988) studied that the design of polymeric composite structures for cold regions applications and found that changes in temperature of composite materials result in two very important effects. First, a decrease in temperature, due to either cooling during the fabrication process or low temperature operating conditions, will cause the matrix to shrink. In fiber reinforced polymer matrix composites, the coefficient of thermal expansion of the matrix is usually an order of magnitude greater than that of the fibers. Contraction of the matrix is resisted by relatively stiff fibers through fiber-matrix interface bonding, setting up residual stresses within the material microstructure. The magnitude of the residual stresses is proportional to the difference in curing and operating temperatures of the composite material. In cold region environments this difference may be as large as 400°F, and residual stresses may be sufficiently large to cause microcracking with in the matrix and matrix-fiber interfaces. A second important effect of temperature change is an accompanying change in matrix strength and stiffness. Most resin materials become stronger and stiffer as they are cooled. Composite material damage usually begins with the formation of microscopic cracks in the matrix or at the matrix-fiber interface. When these cracks develop to a certain density and size, they coalesce to form macroscopic matrix cracks. Transverse matrix cracking in composite laminates has been shown to affect laminate stiffness, strength, dimensional stability (thermal expansion), and fatigue resistance. In addition, such materials subjected to aggressive environments may suffer reduced corrosion resistance due to increased permeability caused by increase in matrix crack density.

The crack growth process described above occurs as stress levels increase due to increases in applied loading and/or due to cooling during the fabrication process itself. A

class of problems where crack growth due to residual stresses becomes very important occurs under cyclic mechanical or thermal loading. Of particular interest here is the case of prolonged low temperature thermal cycling where material damage can grow and accumulate to result in composite material degradation. Low temperature thermal cycling has received much attention by those concerned with composite materials for aerospace application. A review of some of the more pertinent work related to the effects of low temperature thermal cycling on degradation of composite laminates is presented below.

Mazzio et al. (1973), Daniel and Liber (1975), Fahmy and Cunningham (1976), Lundemo and Thor (1977), Givler et al. (1982) considered the effects of moderately low temperature thermal cycling of a variety of composite laminate materials and construction. Unidirectional $[0°]_8$ graphite/epoxy laminates were subjected to thermal cycling from –60°F to 300°F. No noticeable effects were observed during the first 100 cycles. However, after 100 cycles, degradation occurred through delamination. Cracks parallel to the fibers gradually developed, the number of cracks increasing with the number of cycles. Angle-ply laminates of the same material were much more affected by thermal cycling than the unidirectional laminates, and developed transverse matrix cracks in the plies. Cracking was most severe during the first 10 thermal cycles, and then tapered off. Matrix cracks in the plies did not cross adjacent layers. After 100 cycles there was not noticeable delamination.

Also they looked at thermal cycling from –100°F to 72°F, testing cross-ply $[0_2/90_2]_s$ and angle-ply $[0_2/\pm45]_s$ laminates made of boron/epoxy, boron/polymide, graphite/epoxy and S-glass/epoxy composites. In general, the cross-ply laminates were more severely affected than the angle-ply laminates. In addition, graphite/epoxy and S-

glass/epoxy laminates were subjected to a combination of constant tensile load, equal to 60% of ultimate strength, and thermal cycling. Both laminates showed visible degradation. Also hybrid glass-carbon/epoxy laminates were subjected to thermal cycling from –65°F to 350°F. There was some initial ply cracking during the curing process. The crack density increased eightfold during 1000 thermal cycles and the observed cracks occurred in 90° and adjacent ±45° plies.

Givler, Gillespie and Pipes (1982) subjected carbon/epoxy $[(\pm 45)_8]_s$ laminates to thermal cycling that simulated aircraft flight conditions and included thermal spikes and moisture effects. Material property degradation was assessed subsequent to thermal cycling. The effect of moisture plus thermal cycling was to plasticize the composite. Fiber dominated behavior was adversely affected, especially at high temperatures. Static tensile strength decreased with longer exposure, and fatigue properties were significantly reduced.

Camahort et al. (1976), Eselun et al. (1979), Cohen et al. (1984), Bowles (1984), Tompkins et al. (1985), Adams et al. (1986), Hyer (1986), Hyer et al. (1986) looked at the effects of extreme low temperature thermal cycling, which would be expected in space environments or cryogenic applications. In a study of graphite/epoxy and hybrid laminates, all composites showed microcracking after 25 cycles from –320°F to 212°F.The laminates were tested for material property degradation subsequent to thermal cycling. Even though the mechanical properties did not change significantly, there was significant degradation of the coefficient of thermal expansion as well as microyield behavior of the 350°F epoxy-resin laminates, both of which affect the dimensional stability of the composite material. Several studies have considered the effect of thermal

cycling on angle-ply graphite/epoxy tubes, which are important elements in space structures. Eselun et al. (1979) subjected tubing made of (0°/±60°/0°) graphite/epoxy laminates to thermal cycling from –250°F to 75°F in vacuum. In this study about 96% of all cracking occurred during the first cycle. Cohen et al. (1984) cycled graphite epoxy tubes from –250°F to 200°F, and carefully examined after various increments of cycling. In all systems tested, matrix cracking occurred after enough cycles. Crack accumulation appeared to level off after 10-50 cycles, and then increase again after 50-100 cycles. Even with extensive cracking the fiber dominated bending and extensional stiffness of these tubes were not significantly affected, while matrix dominated torsional stiffness was strongly affected.

Cogswell (1992) note that in composite materials the stresses induced by repeated thermal cycling can lead to microcracking and a progressive change in properties. Sykes (1986), Funk (1988) and Barnes (1989) have exposed carbon fiber/PEEK composite to thermal shock, typically in the temperature regime 100°C to -150°C. There was no detectable effect on residual properties, although after 500 cycles some microcracking is observed in such thermoplastic composites. Barnes (1989) indicates that he has been able to thermally shock cross-plied carbon fiber/PEEK from room temperature into liquid Helium up to 1,000 times with out inducing microcracking. Also Sullivan and Ghaffarian (1988) note that Continued thermal cycling results in thermally induced microcracks. Best microcracking resistance occurs with reduced cure temperatures and lower fiber volume with random carbon mat surface piles.

According to Kaw (1997) Mechanical performance of composites is influenced by the presence of microcracks. The interdiffusion of atoms or molecules of the fiber and

matrix into each other at the interface creates a distinct interfacial layer, called the interphase, with different properties from that of the fiber or the matrix. This interphase can cause microcracks in the fiber. These microcracks, reduce the strength of the fibers & hence that of the composite.

2.2 Mechanical properties at low temperature

As the mechanical properties constitute the primary criteria for composites performance, measurements of such properties have been widely used to characterize the extent of degradation upon exposure to various environments. As many structures will work at low temperatures in the future, the material properties at these temperatures are required for design purposes. The most important properties are strength, stiffness and thermal characteristics. The physical properties of materials at very low temperatures differ drastically from those commonly encountered. Hence the effect of cryogenic temperatures on mechanical properties was investigated first.

According to Isaac and Ishai (1994) Interlaminar shear strength is a measure of the in situ shear strength of the matrix layer between plies. There is no method available for exact determination of this property. Approximate values of the interlaminar shear strength, or apparent interlaminar shear strength, can be obtained by various tests. The most commonly used test is the short beam under three-point bending as shown in figure 2.1. The beam is machined from a relatively thick (at least 16 plies thick) unidirectional laminate with the fibers in the axial direction and is loaded normally to the plies (in the 3 direction). But the validity of results obtained from thin laminates (less than 16 plies thick) is doubted because of local compressive failure near the loaded points. Better

results are obtained with thicker laminates, approximately 50-plies thick. Because of its simplicity, the short beam shear test is used as a quality control test of the lamination process and related matrix dominated properties of the composite.

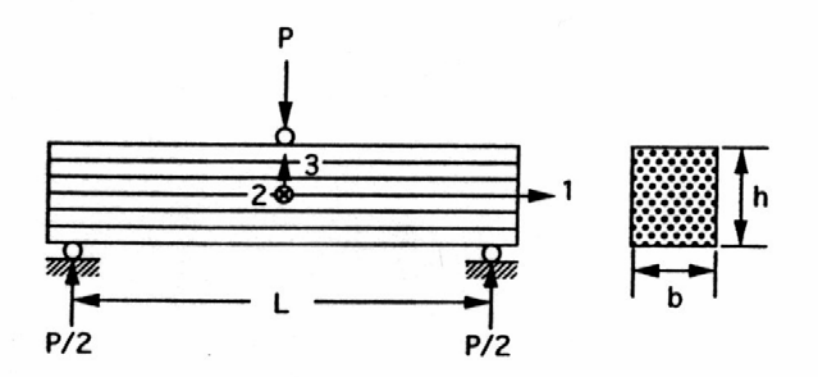

Figure 2.1. Short beam shear test for measurement of interlaminar shear strength.

If the beam is sufficiently short compared with its depth, shear failure will take place at the mid plane in the form of delamination and the interlaminar shear stresses larger than those predicted by classical theory exist. The apparent interlaminar shear strength obtained from classical beam theory is given by

$$F = \frac{3P}{4BH}$$

P→ load at failure initiation

B→ width of beam

H→ depth of beam (laminate thickness)

If the beam is too long compared with its depth, flexural failure (tensile or compressive) may take place at the outer plies of the beam. To ensure interlaminar shear failure prior to flexural failure, the span to depth ratio must satisfy the relationship

$$\frac{2L}{H} < \frac{F1}{F}$$

L→ beam span

F1→ flexural strength of beam in fiber direction

According to Jones (2001) strength is determined by the region of the specimen most affected by exposure to environmental attack. The results of mechanical tests on fiber reinforced polymer samples exposed to environmental degradation by measurements of various physical and chemical characteristics indicate the changes of the structure of composites at the microscopic level.

Weiss (1982) conducted several experiments to find the mechanical and thermal properties. He selected materials with extreme properties since some characteristics of fibers and resins vary considerably. The fibers chosen were the high tensile fiber T300 and the high modulus fiber M40A. The laminates were all unidirectional. The resins selected were semi flexible epoxy CY221/HY979 and rigid epoxy LY556/HY917. The mechanical properties measured were Young's Modulus E, Poisson ratio ν, fracture strain ε_F and fracture stress σ_F. Table 2.1 shows the results.

Resin	Fiber	Temp K	Fiber orientation	E $kNmm^{-2}$	ν [-]	σ_F Nmm^{-2}	ε_F %
CY 221/ HY 979	T300	293	∥	132	0.34	1700	1.22
		77	∥	141	0.32	2010	1.34
	M40 A	77	⊥	11.45	0.012	42.2	0.37
LY 556/ HY 979	T300	293	∥	135	0.31		
		77	∥	137	0.31		

Table 2.1. Mechanical properties of unidirectional laminates at 293K and 77K.

The Young's Modulus parallel to the fibers of the composites with the semi flexible resin (CY221/HY979) and high modulus fiber (M40A) rises from 132GPa at room temperature to 141GPa at 77K, which means an increase of 7%. With rigid resin (LY556/HY917) the rise is only 2%. Poisson's ratio of the semi flexible resin with T300 becomes 6% smaller whereas for the rigid resin it remains constant, when the temperature

is changed from 293K to 77K. The fracture stress of the composite in fiber direction rises from 1700MPa to 2010MPa, which is an increase of 18%. Also the fracture strain is larger at 77K than at room temperature. It rises 10%. The mechanical properties perpendicular to the fiber measured at 77K are low in comparison to those parallel to the fibers. The Young's modulus is only 8%, Poisson's ratio 4%, the fracture stress 2% and the fracture strain 28% of the values parallel to the fibers. However there seems to be a large increase of the values due to temperature decrease. The thermal expansion of semi flexible resin and high modulus fiber is shown in figure 2.2. Most mechanical properties of unidirectional carbon fiber reinforced composites show a higher value at low temperature.

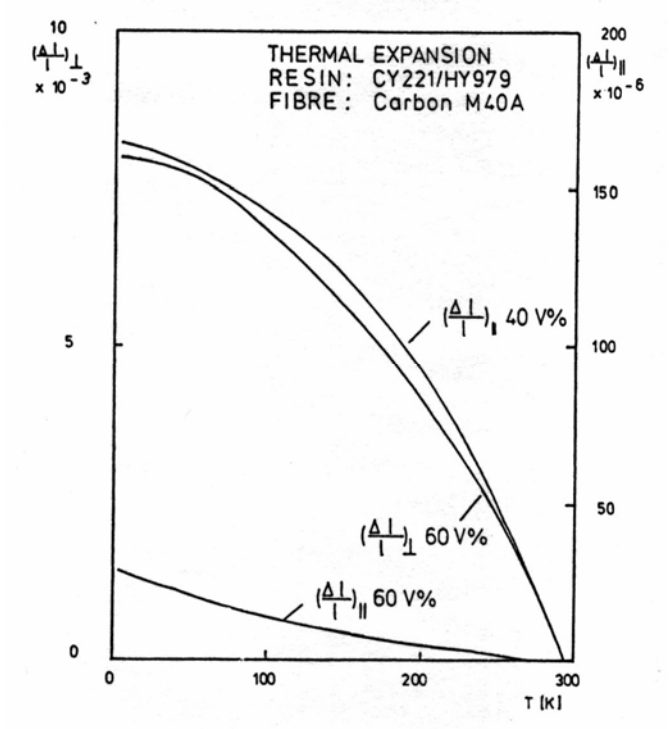

Figure 2.2. Thermal expansion from 293K to 4.2 K

He then conducted tensile and compression tests on graphite/epoxy composites at low temperatures. Figure 2.3 shows that the modulus changed very little with temperature

and tensile strength was maximum at room temperature. Transverse tensile and compression data are shown in figure 2.4 with tensile strength changing only slightly with temperature, while compression strength was maximum at –162°C. He also measured the coefficient of thermal expansion and thermal conductivity at low temperatures as shown in figure 2.5 and table 2.2 respectively.

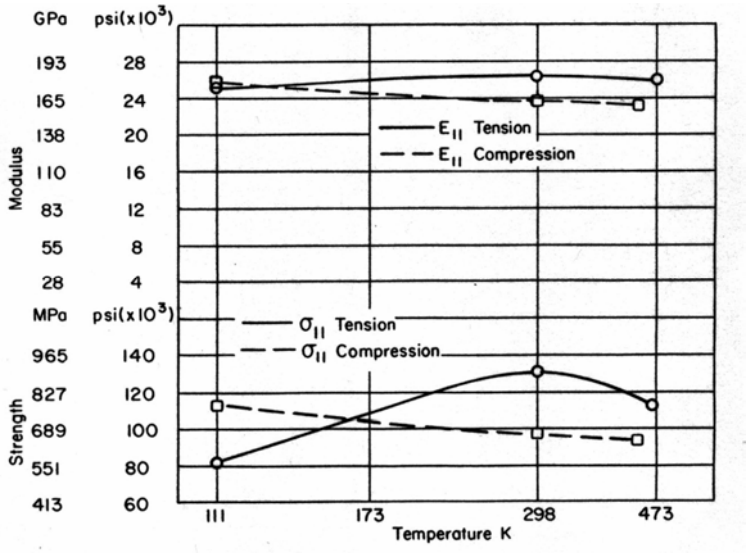

Figure 2.3. AST2002 HMS unidirectional properties versus temperature

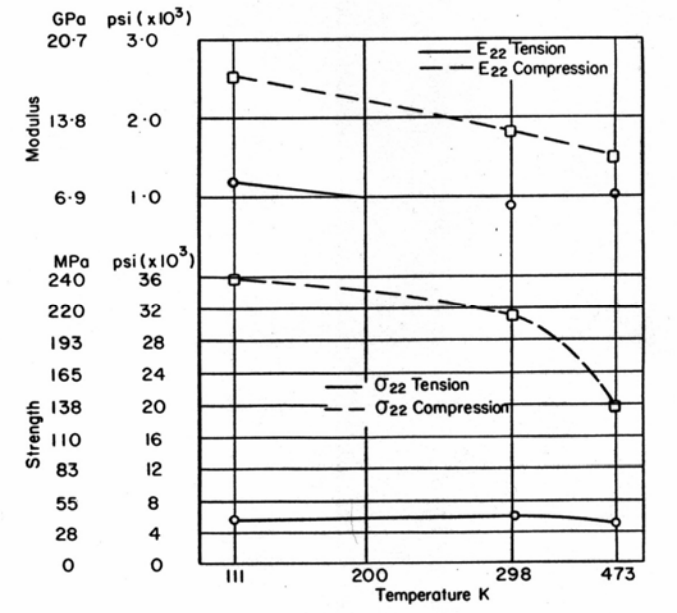

Figure 2.4. AST2002 HMS transverse properties versus temperature

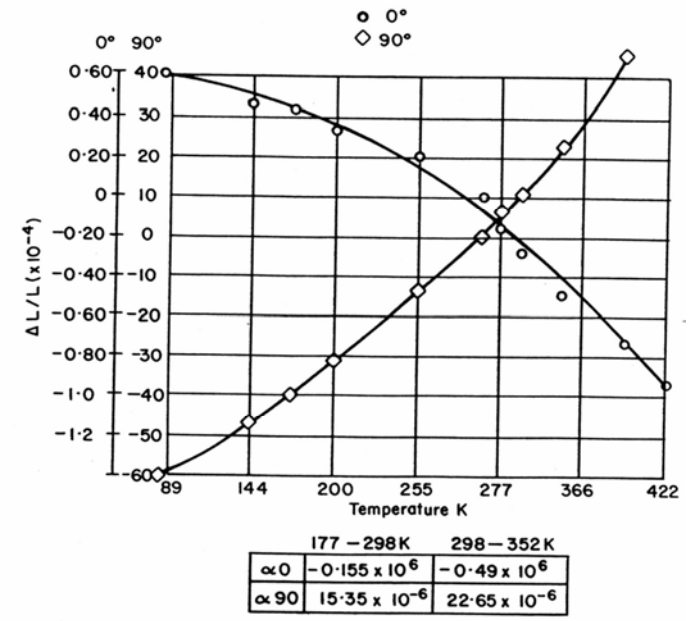

Figure 2.5. 2002/HMS graphite/epoxy thermal expansion data

Mean temperature		Thermal conductivity $wm^{-1}K^{-1}$	
K	ºC	90º Transverse	0º Longitudinal
203	-70	0.69	31.5
253	-20	0.78	35.5
273	0	0.82	37.0
293	20	0.85	38.4
333	60	0.89	41.5
373	100	0.93	44.4
423	150	0.95	47.5
Note: Specimen size 9mm X 63mm X 63mm, average specimen density 1559 kgm^{-3}			

Table 2.2. Thermal conductivity test results

He also found that in-plane shear modulus decreases as temperature increases while interlaminar shear strength remained constant at temperatures less than 25°C as indicated in figure 2.6.

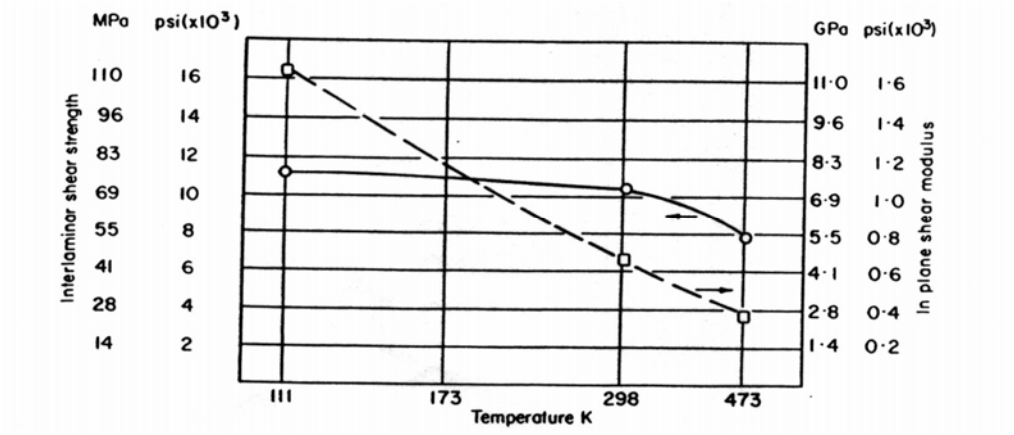

Figure 2.6. AST2002/HMs shear strength and modulus versus temperature

2.3 Acoustic Emission for monitoring microcracks

The concerns regarding the prolonged use of composites is their ability to retain integrity after exposure to thermal cycling, which occurs in applications where cycling between ambient temperatures and cryogenic temperatures is required. For composites the shear strength increases at cryogenic temperatures but due to the difference in thermal expansion coefficient between the matrix and the reinforcement, thermal stresses are induced at decreasing temperatures. These stresses may seriously weaken the interface bonding and thus adversely affect the structural integrity of the composite material. Layered composites may delaminate under thermal cycling. Several damage mechanisms may be present when composite materials are subjected to severe temperature drops or thermal excursions through low temperatures. The damage can occur at numerous locations throughout a composite specimen. Acoustic Emission (AE) monitoring provides a useful tool to monitor these damage occurrences.

AE is classified as a NDT method. It is a useful technique to monitor the damage (number of fiber breaks) during the test, particularly for non-transparent matrix materials. It is based on the phenomenon that the sudden release of energy inside a material results in emission of acoustic pulses. Energy release occurs as a result of deformation or failure processes caused by thermal stresses. The acoustic signals are detected by piezoelectric transducers in contact with the specimen through a coupling medium, electronically processed and recorded. The usual procedure is to count the number of pulses above a preset amplitude threshold. The result can be recorded and presented in terms of a cumulative number of counts, which indicates the extent of damage or rate of counts, which is related to the rate of damage growth. The various mechanisms of failures in composites produce signals of different amplitude. Thus fiber breakage produces a higher A.E. activity than fiber debonding, which in turn produces more measurable counts than matrix cracking.

Instrumented experiments with AE phenomenon were first reported by Fritz Foster and Eric Scheil of Germany in 1936. They recorded the sounds generated by the formation of martensite in nickel steel. Mason, McSkimin and Shockley (1948) performed a second series of experiments utilizing instrumentation in US. Their objective was to record low-level twinning dislocations in tin.

Dutta and Farrell (1988) conducted a series of AE experiments on fiberglass/epoxy and graphite/epoxy laminated composites at low temperatures. The focus was on relating the number of the acoustic events and their amplitudes to the decrease of temperatures of composites. Sufficiently low temperatures can induce numerous damage mechanisms in composites, which include transverse matrix cracking,

debonding, delamination and fiber failure. The damage accumulation was monitored as a function of temperature, which was slowly changed over a period of time (about 30 minutes). The AE signals emitted from the test specimen were measured as the specimen was cooled. The graph of cumulative events versus temperature for fiberglass/epoxy specimen is shown in figure 2.7-2.8 and for graphite/epoxy composite in figure 2.9. Figure 2.10-2.12 shows the typical amplitude distributions of these composites respectively. The cumulative counts of acoustic events increased as the temperature decreased, indicating the progressive development of micro cracks. The number of events is lower for the unidirectional composites than the multilayer laminates. The residual stresses induced in unidirectional laminates are primarily caused by differences in thermal expansion coefficients between the fibers and the matrix. However, in multilayered laminates complex and possibly more severe stress fields are setup because of differences in elastic and hygrothermal properties between the adjacent layers.

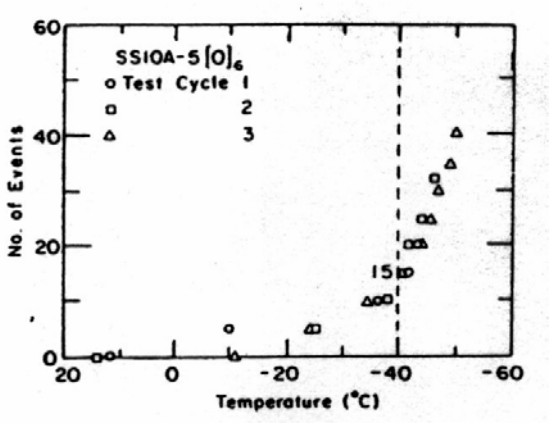

Figure 2.7. AE event counts for glass/epoxy $[0]_6$

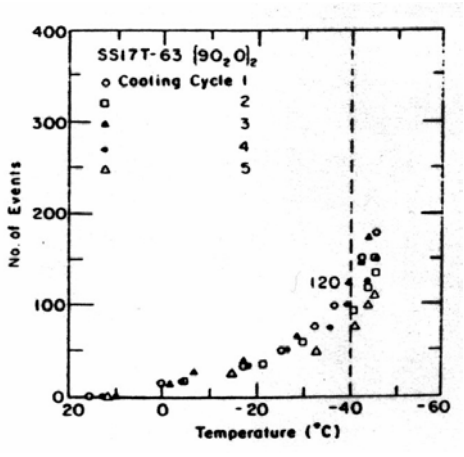

Figure 2.8. AE event counts for glass/epoxy $[90_20]_2$

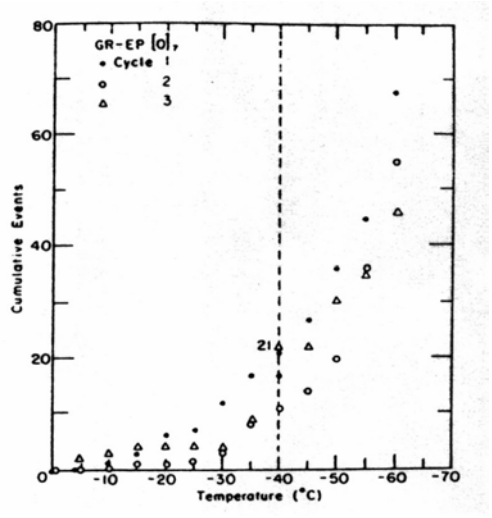

Figure 2.9. AE event counts for graphite/epoxy $[0]_7$

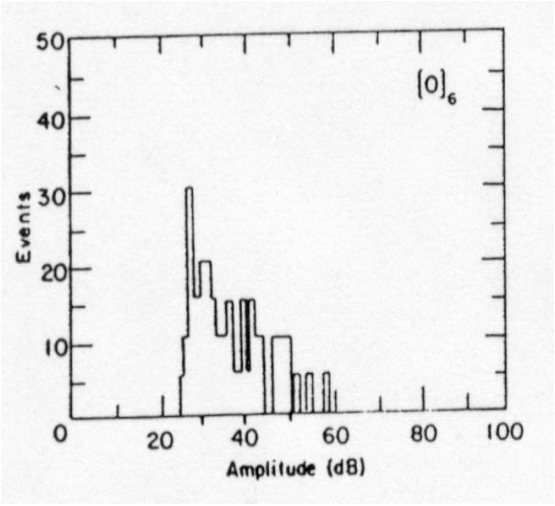

Figure 2.10. Amplitude distribution of glass/epoxy $[0]_6$

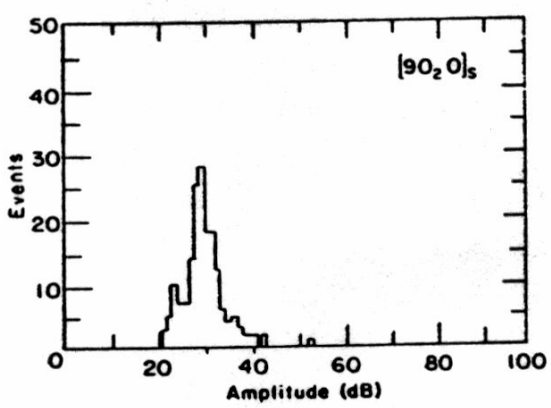

Figure 2.11. Amplitude distribution of glass/epoxy $[90_20]_s$

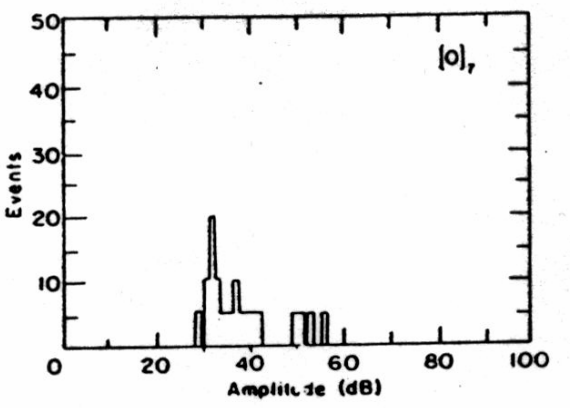

Figure 2.12. Amplitude distribution of graphite/epoxy $[0]_7$

Dutta et al. (1988) also investigated whether the development of microcracks and progressive damage accumulation reduces the strength of the laminates. Low temperature thermal cycling of unidirectional laminates of the graphite/epoxy composites with fibers oriented in the direction of applied load, figure 2.13, did not show any degradation in

strength after thermal cycling. In fact, the strength shows an increase by about 9.2%. Whereas a decrease in strength after thermal cycling is noted in multilayered laminates of glass/epoxy composites, figure 2.14.

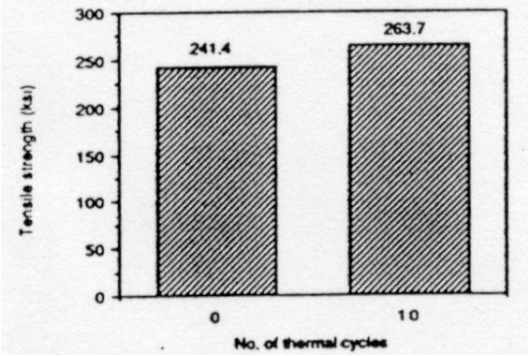

Figure 2.13. Tensile strength of Graphite /epoxy $[0]_7$

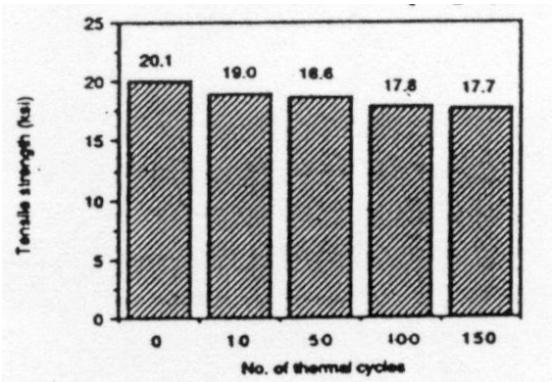

Figure 2.14. Tensile strength of Glass/epoxy $[90_20]_s$

Also according to Kageyama K., (1989) AE wave is an elastic wave corresponding to the microfracture of composites, i.e. matrix cracking, fiber debonding, fiber breakage, and delamination. AE source wave can be characterized as an impulse with wide frequency band, but the AE wave detected by the transducer is little different from the source wave. Frequency characteristics of the transducer and material have a direct effect upon the detected AE waveform. Propagation of AE wave is divided into three classes, i.e., longitudinal (L), side (S) and surface (R) waves, as shown in figure 2.15. The propagation velocity differs for each wave. As a result of superimposition of L, S, R waves, the detected AE waveform is very complicated and quite different from the source wave, which has an impulsive profile.

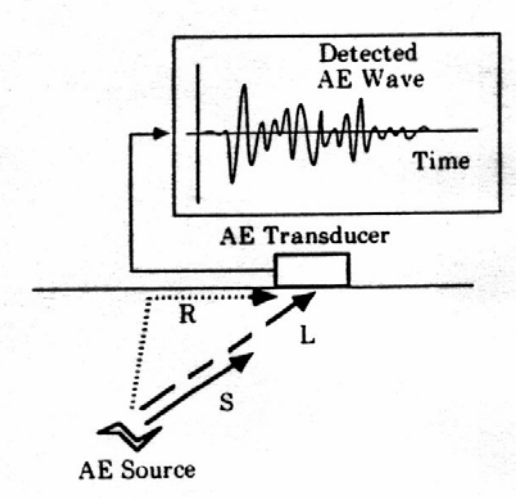

Figure 2.15. Propagation modes of AE wave

As early as 1971, Mehan and Mullin (1971) reported that each different failure mechanism such as fiber fracture, matrix fracture, or debonding had different characteristic acoustic emission signal signatures. Speak and Curtis (1974) concluded that the observed frequencies in the AE signals depended on the material type and geometry but the higher frequencies began to appear as fracture loads were approached. More recent work has indicated that the signal frequencies contain almost exclusively natural frequency components of the specimen transducer system. Investigations are still going on in attempts to make sense of the information contained in the AE signal characteristics. Guild (1980) has pointed out that no simple correlation can in general be expected as, for example, the amplitude of a fiber failure event depends upon the condition of the local fiber fracture site, and a number of other possible factors. Sundaresan and Henneke (1989) suggested a proof test procedure for assessing the fatigue durability of a complex structural member made of carbon fiber thermoplastic matrix composite material. The method is based upon the Felicity ratio, which was introduced by Fowler (1979). The felicity ratio is defined as the load at onset of AE

activity divided by the maximum load previously applied to the specimen. The suggested proof test involved a combination of fatigue cyclic and static tensile loads applied to the structure. This proof test was found to provide an accurate indication of the fatigue life of the composite as shown in figure 2.16.

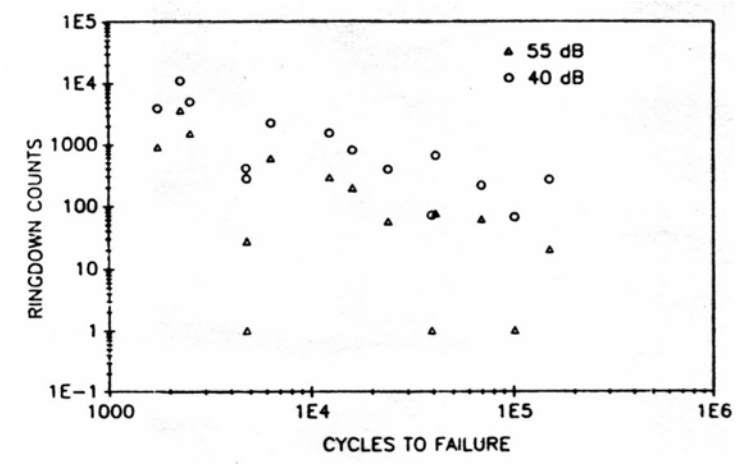

Figure 2.16. Correlation between ring down counts and cycles to failure in a geometrically complex graphite epoxy structure

Mathews and Rawlings (1994) suggested that the simplest method of obtaining an indication of acoustic emission activity is to count the number of amplified pulses which exceed an arbitrary threshold voltage V_t. This is ring-down counting and the signal in figure 2.17 would correspond to twelve ring-down counts. As the signal shown was produced by a single surface displacement it is sometimes convenient to record a count of unity rather than the multiple count obtained by ring-down counting. This mode of analysis is known as event counting. Williams and Reinfsinder (1974) found that the counting techniques are extremely sensitive and are capable of detecting early stages of damage in composites under static and dynamic loading. The counting techniques are found to be particularly useful in the proof testing of PMC (polymer matrix composite) Structures in conjunction with Felicity ratio. Fowler and Gray (1979) found that if the

load is removed during a proof test and then the structure reloaded, emissions may be detected at loads below that previously attained. Refer figure 2.18. The Felicity ratio is a measure of the damage to the composite. The lower the felicity ratio, the greater the damage.

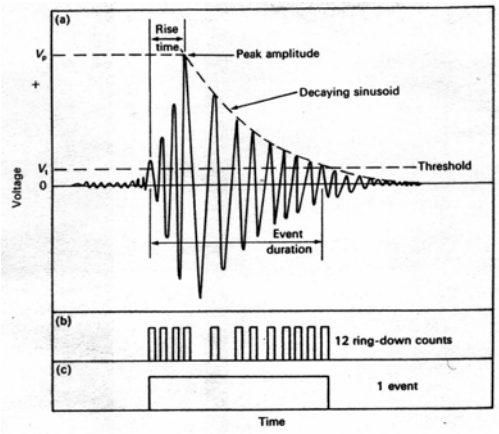

Figure 2.17. Different AE monitoring methods

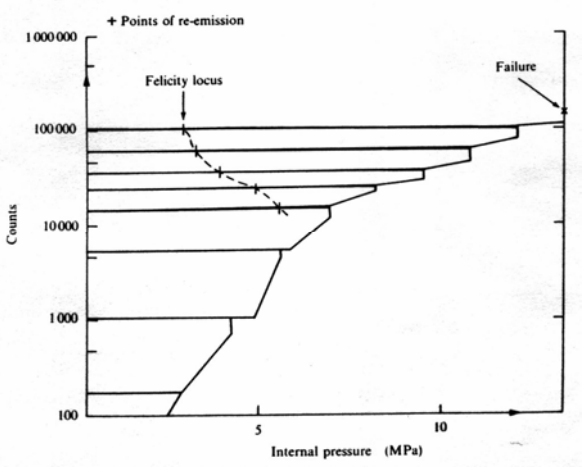

Figure 2.18. AE monitoring of a proof test on GFRP pipe work showing a decreasing felicity ration with increasing load

Again Mathews and Rawlings (1994) proposed that counting techniques are simple and sensitive to damage but, as a general rule, are not good guide to the type and extent of damage. More detailed and comprehensive information on the emissions emitted over a period of time may be obtained from histograms of the number of events against peak voltage and number of events against event duration or pulse width. The peak voltage histogram, also called amplitude distribution, from a composite is usually complex, consisting of a number of peaks each attributed to a particular micro-damage mechanism. Berthelot and Billand (1983) demonstrated how amplitude distributions are an aid to the determination of the extent of the different micro-damage mechanisms as

load is increased. High amplitude events are indicative of high energy, deleterious damage.

A useful review of use of AE techniques in the investigation of polymer based composite materials has been given by Sims (1976) and also Rotem (1977). The acoustic emission trace shown in figure 2.19 is characteristic of microfracture in composite materials. There is a rapid increase in the number of noise producing events as the strain increases beyond the knee indicating that further cracking is occurring.

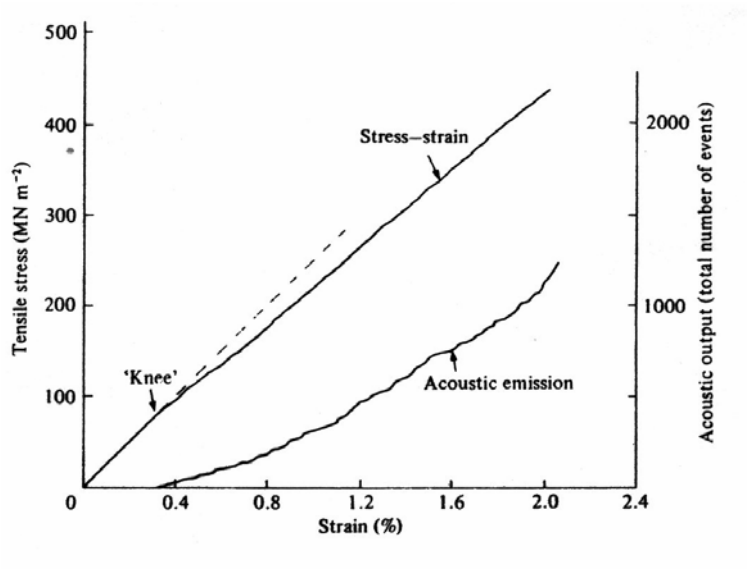

Figure 2.19 Stress strain curve and acoustic emission output of a cross ply laminate in uniaxial tension

2.4 Permeability

Composite laminates are commonly used as various structural components and the major candidates for reducing the structural weight of the reusable launch vehicles (RLV). Especially, application of CFRP laminates to the cryogenic propellant tanks is

one of the most yearning but challenging technologies for achieving the drastic weight reduction of RLV. Recent basic studies by Aoki et. al (2000) and Kumazawa et. al (2001) on the feasibility of composite liquid propellant tanks indicated that matrix crack onset and its accumulation is inevitable when applying the conventional high performance composites to the cryogenic tanks and multi laminar matrix cracks may induce crucial propellant leakage. Thus the adequate guideline for possible application of CFRP laminates to the propellant tanks is necessary from the leakage and damage tolerance point of view. Damage in cryogenic composite fuel tanks induced during manufacturing and advanced by thermo-mechanical cycling can accelerate leakage of the propellant. Whether the leakage exceeds tolerable levels depends on many factors, including pressure gradients, microcrack density, other damage such as delamination, connectivity of the cracks, residual stresses from manufacture, service-induced stresses from thermal and mechanical loads, and composite lay-up.

Morse, Ochoa and Barron (1992) found that the Flow in different directions of the same material could produce different values of permeability. It is therefore important to note the direction of flow associated with a given permeability. The permeability of a given material is usually given in terms of the Darcy permeability. The Darcy permeability is defined as:

$$D = \frac{flowrate \times vis\cos ity \times thickness}{differentialpressure \times area}$$

This permeability value is a function to the material alone, and not a function of the flow conditions. They conducted experiments to find the z, x, y permeabilities for a number of materials keeping the same differential pressure (150 psi). The flow medium

used in testing was Terrasic 68, a turbine oil with room temperature viscosity of approximately 134 cp. The z-permeability is defined as the resistance of a material to fluid flow perpendicular to the material plane. x-permeability and y-permeability will correspond to flows in the 0 degree and 90 degree fiber directions respectively. The z-permeability of the various layers and layer combinations was determined using a fixture shown in figure 2.20. The z-permeability machine holds a sample disk of the material in a cylinder through which a viscous medium flows. The material sample is held between two porous plates, separated by a spacing ring, so that its thickness remains constant, independent of the flow rate. By carefully measuring the flow rate, pressure drop across the sample, sample thickness, and the viscosity of the flow medium, a value for the permeability of the material was obtained. Both x and y permeabilities were also obtained.

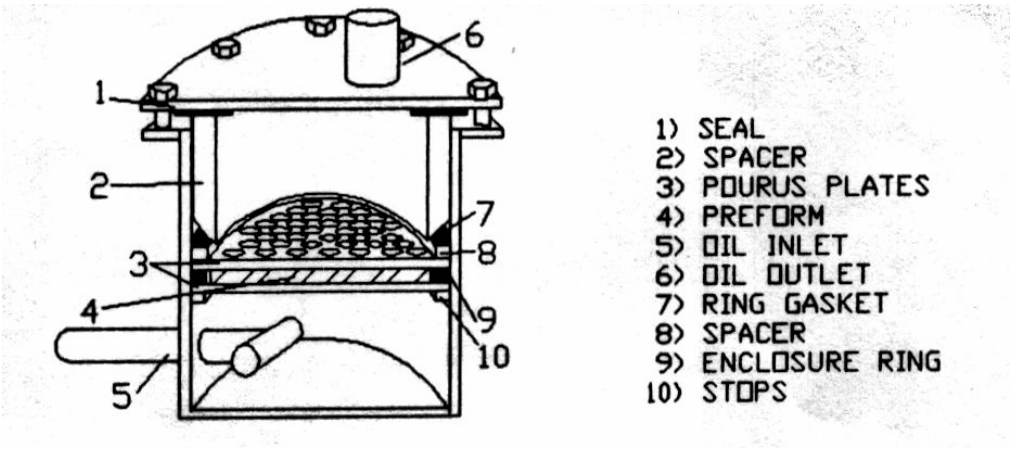

Figure 2.20. Permeability test fixture

They observed that initially permeability decreases with increasing flow rate, which holds true only for the first time a material is subjected to a given flow rate. This decrease in permeability is attributed to a geometric change in the material as the various fiber bundles began to nest together with increased differential pressure across the

specimen. Thereafter if the flow rate is reduced then brought up again, the permeability remains relatively constant. Figure 2.21 shows the dependence of permeability on flow rate for a certain material. Table 2.3 shows the results of their experiments. They also observed that several of the materials appear to be approaching a minimum value of permeability asymptotically as flow rate increases, thus a minimum "limit" value for the permeability of these materials can be set.

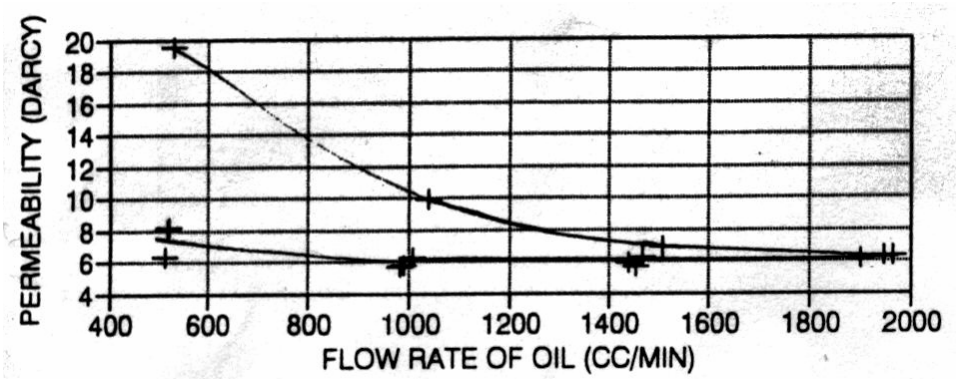

Figure 2.21. Permeability Vs flow rate

Material #	Fiber weight %		Permeability (Darcy)	
	6.0 mm	4.7 mm	6.0 mm	4.7 mm
1	52	60	5.0	4.0
2	60	70	3.0	1.8
3	52	60	25.0	20.0
4	60	70	10.0	8.0
5	60	70	8.0	3.0
6	60	70	5.0	2.5
7	60	70	0.8	n/a
8	60	70	19.0	7.0

Table 2.3. Permeability results

Units of permeability:

The units of permeability are expressed in different ways by several authors. According to Turner (1979) the units of permeability are as below.

Nomenclature: m-meter; s-second; N-newton; kg-kilogram; cm-centimeter; g-gram; lbf-pound; ft-foot; in-inch; mol-mole; Pa-pascal.

SI units:

$$D = \frac{\eta Q h}{A \Delta P}$$

where D= permeability of the material

η= viscosity of the gas/fluid (Ns/m^2) or (kg/ms)

Q= rate of flow of gas/ fluid (m^3/s)

h= thickness of the sample in the direction of flow (m)

A= surface area of the sample (m^2)

ΔP = pressure difference measured across the sample (N/m^2) or (kg/ms^2)

and $D = \frac{Ns/m^2 * m^3/s * m}{m^2 * N/m^2} \Rightarrow D = m^2$

or $D = \frac{kg/ms * m^3/s * m}{m^2 * kg/ms^2} \Rightarrow D = m^2$

Metric or CGS units:

η= centipoise or (g/cms)

Q= cm^3/s

h= cm

A= cm^2

ΔP = bar or g/cms^2

and $D = \frac{g/cms * cm^3/s * cm}{cm^2 * g/cms^2} \Rightarrow D = cm^2$

FPS units:

η= $lbfs/ft^2$

$Q = ft^3/s$

$h = ft$

$A = ft^2$

$\Delta P = lbf/ft^2$

and $D = \frac{lbfs/ft^2 * ft^3/s * ft}{ft^2 * lbf/ft^2} \Rightarrow D = ft^2$

According to Evans and Reed (1998) permeability can be referred as the passage of gas through a resin/composite barrier and is defined as below:

$$Permeability = \frac{dn}{dt} \times \frac{h}{A\Delta P}$$

where dn/dt = amount of gas passing through the plate (mol/s)

h= plate thickness (m)

A= surface area (m^2)

ΔP= pressure difference (bar)

Hence the permeability has the units of mol/smbar. However if the quantity of gas (mol) is expressed as m^3 and the pressure in Pa or N/m^2, the units become m^4/sN. Disdier et al. also expressed permeability in terms of mol/smPa. Jens Humpenoder (1998) expressed permeability as m^2/s.

According to Whitcomb (2002) the diffusion of gases in composites is not important, but the leakage resulting from flow through interconnected cracks is expected to be the major factor. He studied the permeability of flow of liquid hydrogen through a single crack. Flow of liquid hydrogen in a sample crack in a 90 Ply was analyzed using FLUENT, a Computational Fluid Dynamics software. Figure 2.22 shows the 2-D representative volume element (RVE) containing a single crack of the IM7/5250-4

composite specimen, subjected to uniaxial tensile stress of 100MPa. Figure 2.23 shows the geometry of the crack. The density of the liquid hydrogen used was 0.08189 Kg/m3 and viscosity was 8.411E-6. The geometry of the crack does not allow for any fluid flow in the horizontal direction. Following a standard homogenization procedure a boundary value problem with given pressure difference between the top and bottom of the crack and no slip boundary conditions at the walls of the crack was solved and a 2-D permeability tensor was found. Comparing this value with the analytical value for a straight channel of the same width and height, the difference in the permeability constant was found to be 30.4%. Based on this it is concluded that the study of flow through the cracks will require the actual crack shape.

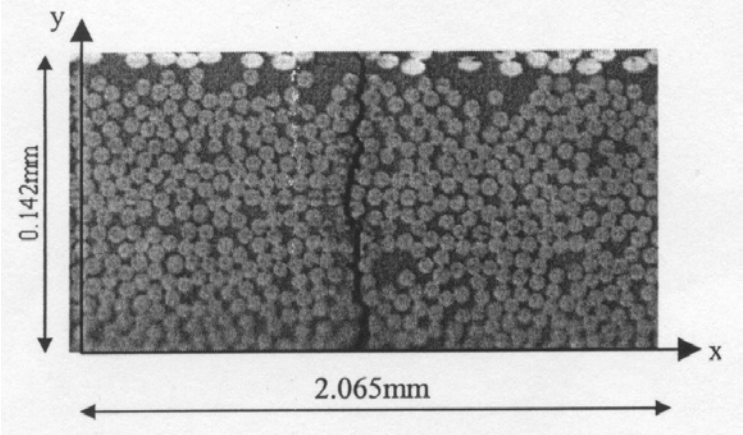

Figure 2.22. Representative volume element in the composite

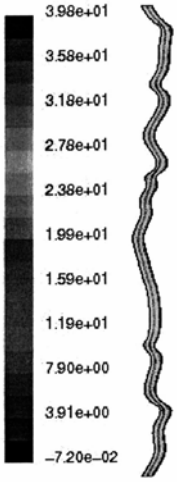

Figure 2.23. Contour plot of the y-component of velocity (m/s)

According to Cogswell (1992) there can be resin percolation both along and across the fibers as shown in figure 2.24. He also concluded that the description of such percolations could be made in terms of the Darcy Permeability Coefficient.

The Darcy Permeability Coefficient = $\frac{\text{viscosity x mean velocity x thickness}}{\text{Pressure drop}}$

There are several analytical and experimental studies of resin permeability in fiber beds. Analytical studies by Cogswell (1987) and Wheeler (1990) indicate that the permeability along the fiber direction is significantly greater than that through the thickness. The permeability is higher with large diameter fibers: large fibers. Larger holes, easier flow. The permeability decreases by approximately one order of magnitude as fiber volume fraction increases from 55% to 65% by volume.

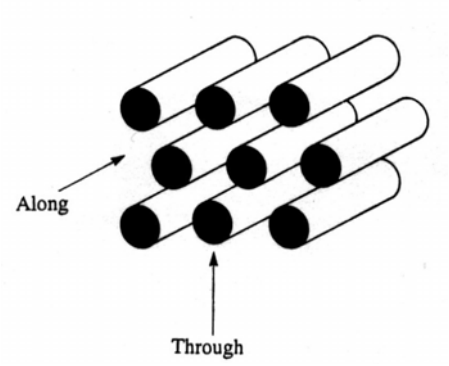

Figure 2.24. Anisotropic permeability

Wheeler (1990) notes that transverse permeability is not significantly affected by local fiber organization at those high volume fractions. Lam and Kardos (1988) have made direct measurements of axial and transverse permeability of carbon fibers, using viscous oils. Those results, shown in table 2.4, are in satisfactory agreement with the analytical predictions. The permeability through a stack of plies of different orientation is reduced in comparison with that through a uniaxial laminate. Resin rich layer concentrates the fibers more densely in the center of the ply and denser array is of lower permeability. Lam and Kardos (1988) indicate that, if the plies are at an angle of 45°, permeability is reduced by 25%, and for cross-plied laminates the reduction is 50%. The permeability coefficient is determined by geometric constraint of the fiber bed.

Permeability coefficient (m^2)				
Volume fraction %	Analytical solution		Experimental results	
	Axial	Transverse	Axial	Transverse
50	4.5×10^{-13}	1.8×10^{-13}	5.8×10^{-13}	1.4×10^{-13}
55	3.5×10^{-13}	1.0×10^{-13}	3.1×10^{-13}	0.9×10^{-13}
60	2.3×10^{-13}	0.5×10^{-13}	1.9×10^{-13}	0.5×10^{-13}
65	1.5×10^{-13}	0.2×10^{-13}	1.0×10^{-13}	0.3×10^{-13}

Table 2.4. Permeability of carbon fibers by viscous resins

Evans (1988) has studied the permeability of carbon fiber/PEEK composite to hydrogen in the temperature range of 25 to 60°C, as shown in table 2.5. It takes about 3 days to establish equilibrium permeability of this gas through a 2mm thick sheet of composite. Evans (1989) notes that this value was unaffected by thermal cycling, confirming the strong resistance of these materials to microcracking. He concluded that the results were as good as could be expected for a well-bonded composite. It is possible to conclude that any diffusion process that occurs in a well-made thermoplastic composite will be at the molecular scale rather than exploiting major faults in the material.

Temp°C	Permeability Mol/ms bar
25	7.2×10^{-12}
40	9.4×10^{-12}
60	15.1×10^{-12}

Table 2.5. Permeability of carbon fiber/PEEK composite to hydrogen (2mm thick quasi-isotropic sheet)

Nishijima, Okada, Fujioka, Kuraoka (1988) and Evans, Morgan (1984) has shown that Helium permeation can be expressed by an Arrhenius equation. The data extrapolated to liquid helium temperature would give a negligible permeation rate.

Consequently, if a fiber reinforced polymer shows gas leakage at low temperatures, it is attributed to cracking and thermal stresses. Also Will (1994) and Rey, Gallet, Baze and Bunsell (1992) have reported that FRP materials did not show leaks at any temperature and no significant changes of permeation performance after several thermal cycles between liquid nitrogen temperature and room temperature (RT). Moreover, an increase of glass fiber content leads to an increase of mechanical properties and decrease of gas permeation at RT.

Disder, Rey, Pailler, Bunsell (1997,1998) studied the permeability of Helium gas through the glass fiber composites at RT before and after damage caused by thermal shock and tensile loading. They developed a special experimental leak detector equipment to measure the permeation rate and damage developed by thermal cycling in the range of RT to 77K and by tensile tests at RT and 4.2K. They also studied the effects of glass fiber content on permeation rate. Tensile tests producing damage at RT showed different effects on permeation flow of He, caused by cracking. At 4.2K, the limit for using this material is given by matrix cracking. The glass fiber volume fraction is preponderant in controlling the coefficient of He permeation.

The apparatus for measuring low helium leakage rate is shown in figure 2.25 and the permeation cell in figure 2.26. The helium flow was determined by measuring the pressure of helium across a diaphragm.

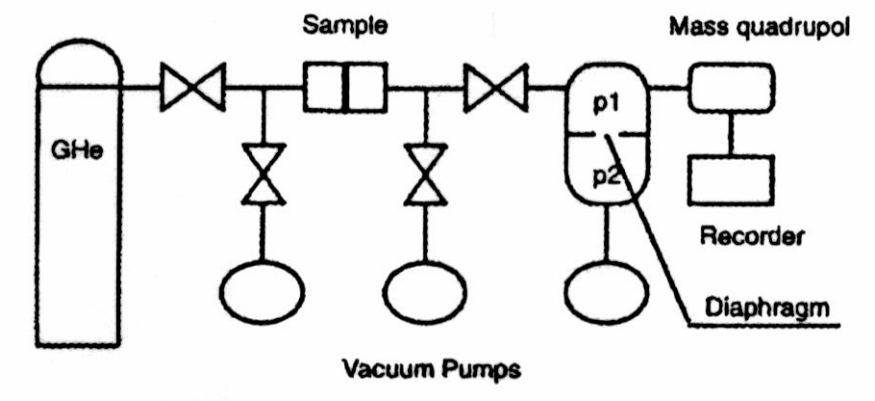

Figure 2.25. Apparatus of helium permeation measurement

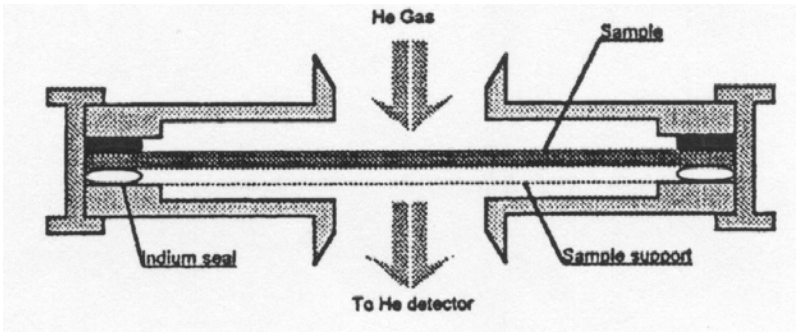

Figure 2.26. Details of permeation cell

The permeation experimental procedure was to introduce the disk into the cell and develop a vacuum so as to be able to connect the mass spectrometer. This process allows elimination of the out gassing problem during the measurement. After the He was introduced, permeation was measured until steady state conditions. All data was recorded on a computer provided with a data acquisition card. The tensile testing procedure consisted of a tensile test to a limited stress after an initial permeation test. This was followed by subsequent tensile tests in which the sample was stressed again to higher levels and the permeation was measured again.

The temperature dependencies of the permeation, diffusion and solubility were measured in the range from 260 to 350K on Vetronite (U11) specimens. The results are

shown in table 2.6. U11 and Prepreg Brochier (PrP) Samples were exposed to thermal cycles. The permeation was measured at RT before and after 50 and 100 thermal shocks from RT to 77K. The effects of thermal damage caused by the differences of thermal expansion rates between the resin and fibers can break the bond and cause a formation of micro cracks. At cryogenic temperatures this effect is enhanced. But they observed that the thermal shocks at 77K had no noticeable effects on permeation, solubility and diffusion rates at RT. Therefore, micro cracking caused by thermal expansion rate differences of the constituents has no detectable effect and the specimens conserve their permeation performance. The results of permeation tests, with and without mechanical damage, are shown in table 2.7 for U11 and PrP specimens at RT and table 2.8 for U11 specimen at 4.2K. For damage provoked at RT, at 84% of failure stress, there is an increase of permeation rate. For lower stresses, no effect has been detected on the helium flow.

Temp©	-15	-10	25	35	45	80
Solubility mol $m^{-3}Pa^{-1}$	$2.6*10^{-6}$	$2.4*10^{-6}$	$2.5*10^{-6}$	$2.3*10^{-6}$	----	$3.5*10^{-6}$
Diffusion m^2s^{-1}	$4.9*10^{-12}$	$6.6*10^{-12}$	$2.2*10^{-11}$	$3.0*10^{-11}$	----	$1.0*10^{-10}$
Permeability mol $s^{-1}m^{-1}Pa^{-1}$	$1.3*10^{-17}$	$1.6*10^{-17}$	$5.5*10^{-17}$	$7.1*10^{-17}$	$1.1*10^{-16}$	$3.4*10^{-16}$

Table 2.6. Temperature dependence on the permeability, diffusion and solubility

Specimen	U11			PrP		
% Failure stress	0	76	84	0	35	44
Solubility mol $m^{-3}Pa^{-1}$	$2.7*10^{-6}$	$2.2*10^{-6}$	$2.1*10^{-6}$	$8.4*10^{-6}$	$1.2*10^{-5}$	$1.4*10^{-5}$
Diffusion m^2s^{-1}	$2.1*10^{-11}$	$2.4*10^{-11}$	$3.0*10^{-11}$	$7.4*10^{-12}$	$5.6*10^{-12}$	$5.0*10^{-12}$
Permeability mol $s^{-1}m^{-1}Pa^{-1}$	$5.6*10^{-17}$	$5.3*10^{-17}$	$6.4*10^{-17}$	$5.6*10^{-17}$	$6.5*10^{-17}$	$6.7*10^{-17}$

Table 2.7. Results of permeation test after mechanical damage at room temperature on U11 and PrP samples

Also the permeation tests at RT were conducted in the range of samples with different weight fraction of glass fiber, the results shown in table 2.9. This indicates that with increasing volume fraction of the glass fibers decreases the helium permeability rate. The lowest permeability is given when the specimen contains 100% glass.

Loading level	0	157	230
% Failure stress	0	340	44
Solubility mol $m^{-3}Pa^{-1}$	$2.3*10^{-6}$	$2.7*10^{-6}$	----
Diffusion m^2s^{-1}	$2.3*10^{-11}$	$1.9*10^{-11}$	----
Permeability mol $s^{-1}m^{-1}Pa^{-1}$	$5.2*10^{-17}$	$5.3*10^{-17}$	$1.2*10^{-14}$

Table 2.8. Results of permeation test after mechanical damage at 4.2K on U11 specimen

Volume fraction of glass (%)	25	35	53	65
Density (g cm^{-3})	1.57	1.87	1.95	2.1
Permeability mol $s^{-1}m^{-1}Pa^{-1}$	$1.1*10^{-16}$	$6.7*10^{-17}$	$2.5*10^{-17}$	$1.6*10^{-17}$

Table 2.9. Permeation dependence on weight fraction.

Yokozeki, Aoki and Ishikawa, (2002) investigated the diffusion controlled gas permeation through CFRP laminates for the feasibility of composite propellant tanks. Using helium gas and a helium leak detector, through the thickness, gas permeability in CFRP laminated tubes with or without matrix cracks was measured at room temperature. Helium diffusion properties through undamaged laminates were obtained to provide basic information of permeability. In order to evaluate the effects of damage and loads on the gas permeability, helium permeation was measured under three conditions: 1) under tensile or compressive loadings without matrix cracks, 2) with matrix cracks alone, and 3) under tensile or compressive loadings with matrix cracks. The material used was carbon/epoxy composite (IM600/Q133) and all tests were conducted at RT.

The Helium permeation test apparatus used is shown in figure 2.27. Helium gas was supplied from the outside of gauge sections wrapped with polyethylene film. The helium leak flux into the inside of tubular specimens was measured with the helium leak detector. They have used the Fick's law with appropriate boundary conditions which was expressed in the form of infinite series as

$$Q = Q_o \frac{\sqrt{4h^2}}{\sqrt{\pi Dt}} \sum_{m=0}^{\infty} \exp\left(\frac{-h^2}{4Dt} (2m+1)^2 \right)$$

Q, Qo= helium leak flux at time 't' and steady state

h= Sample thickness

D= diffusion coefficient

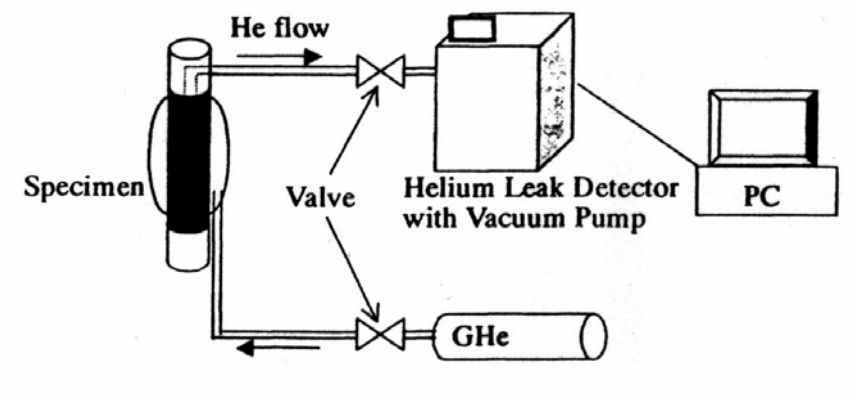

Figure 2.27. Helium permeation test apparatus

For measurement of helium permeation under tensile or compressive loadings, helium was diffused through tubular specimens without loadings to the steady state at first, and then tensile or compressive loadings were applied to the specimens using Instron 4505 testing machine. Tensile or compressive loadings were applied in incremental steps with 10 minutes for keeping the loads constant. Thus, the helium leak flux was measured as a function of applied loads.

Measured helium leak flux through a tubular undamaged specimen without any load as a function of time is shown in figure 2.28. Then the effect of applied loadings on helium leak flux in undamaged specimen was investigated. Figure 2.29 shows the relationship between applied loadings and helium leak flux. As applied loads increase, helium leak flux increases, whereas leak flux decreases under compressive loadings. The helium leak flux reverts to the same value when removing the applied loads, even though it exhibits some hysteresis.

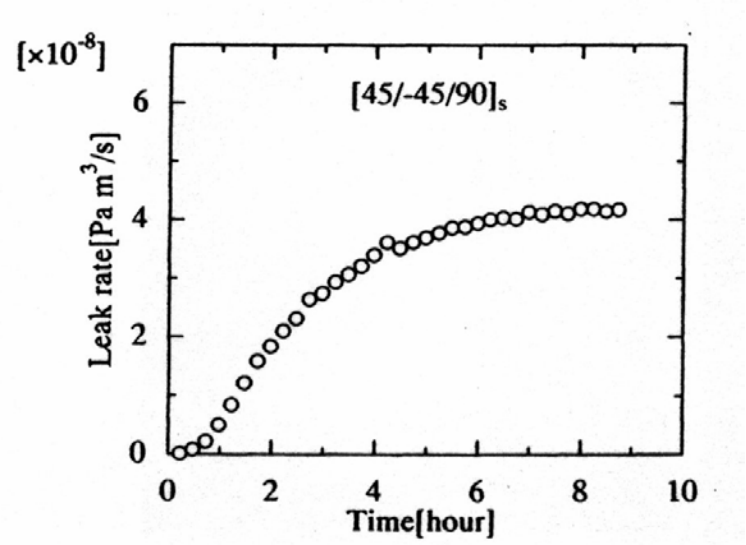

Figure 2.28. Helium leak flux as a function of time through undamaged $[45/-45/90]_s$ tube

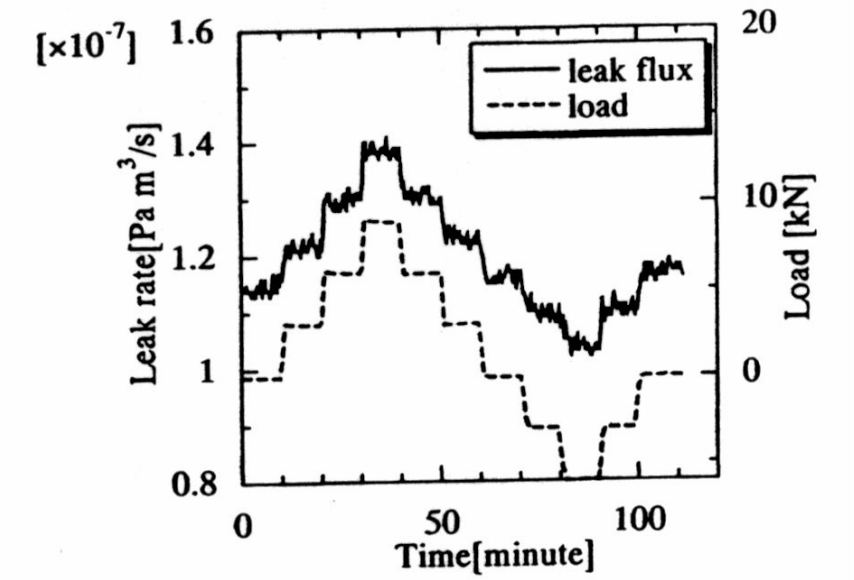

Figure 2.29. Relationship between applied loadings and leak flux of a $[90_2/0/90_2]$ tube.

Considering the case of multi laminar matrix cracks in CFRP laminates, which induce crucial increase of leak flux, the effect of applied loadings on diffusion controlled gas permeability is negligible. Measured helium leak flux through a specimen with matrix cracks is compared with that through undamaged tube in figure 2.30. The relationship between the applied strains and helium leak flux of a cracked specimen is

shown in figure 2.31 in comparison with the data of an undamaged specimen. The existence of matrix cracks leads to an increase of gas permeability under the same loading conditions and higher hysteresis.

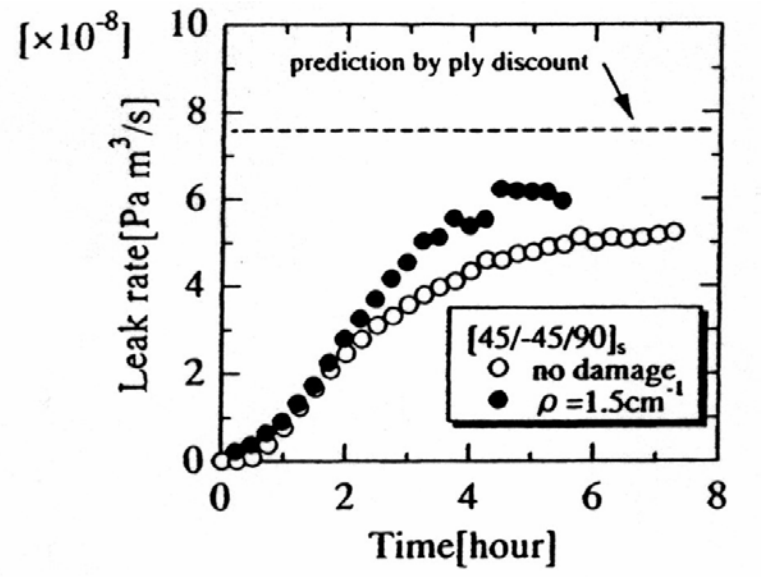

Figure 2.30. Comparison of leak flux between uncracked and cracked $[45/-45/90]_s$ tube.

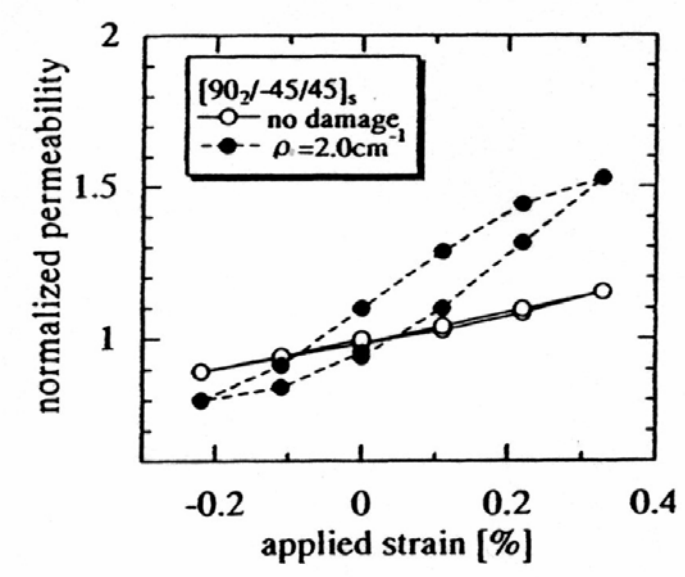

Figure 2.31. Relationship between applied strains and leak flux of a $[90_2/-45/45]_s$ tube with and without matrix cracks

It is concluded that the gas permeability is doubly affected due to both matrix cracks and loads. However, the effect is not crucial, unless specimen have multi laminar cracks, through which the leakage is three or four orders higher than the diffusion controlled permeation. Hence the existence of no less than one intact layer is important for suppression of the crucial propellant leakage.

Hatta, Nishiyama, Bando, Shibuya and Kogo (2002) examined gas leakage through carbon fiber reinforced carbon matrix composites, C/Cs, to find the feasibility of C/C application to heat exchangers in an engine system for a reusable space plane. Gas leakage rates were measured as a function of pressure for various C/Cs and gas flow path was identified by micro observation of the C/Cs. Since C/Cs includes many cracks and pores, gas easily leaks through C/Cs. In order to minimize the gas leak, they impregnated Si into the transverse cracks in a C/C and also coated Si over the surface of a C/C. They observed that the Si impregnation reduces the leak rate by 3 orders of magnitude. However, the Si coating includes many cracks due to thermal mismatch strain between the coating and substrate C/C. So they concluded that the impregnation of Si was effective and the coating was inappropriate.

Hirohata et. al studied the permeability of helium gas in SiC/SiC composite material by using a vacuum apparatus. They carried out the measurement of permeability coefficient of helium gas with pressure ranging from 10^2 to 10^5Pa at RT. The permeability coefficient of SiC/SiC composite largely depended on the preparation method. They observed that in SiC/SiC composite made by both polymer impregnation and pyrolysis (PIP) and melt infiltration (MI) methods showed the lowest permeability, $9.1*10^{-7}$ m^2/s, which was approximately two orders of magnitude smaller than one of the

material made only by PIP method. The permeability of the flat plate SiC/SiC composites made by improvement of the fabrication by both liquid phase sintering (LPS) and hot pressing (HP) was even low, $1.5*10^{-9}$- $4*10^{-11}$ m^2/s. The difference of permeability was related to the microscopic structure, i.e. pores and cracks.

3. Experimental Methodology

Experiments were conducted at US Army Cold Regions Research and Engineering Laboratory (CRREL), Hanover, New Hampshire, for (a) finding effect of temperature on the shear strength of GFRP and CFRP composites, (b) monitoring the microcracks generated in CFRP composite samples due to exposure to cryogenic temperatures using acoustic emission technique and (c) developing a conceptual design for an apparatus to measure the permeability of composites at cryogenic temperatures.

3.1. Short beam shear testing

3.1.1. Experimental Setup

The interlaminar shear strength of the composites was tested using the ASTM D2344-95, short beam shear testing method. The test samples of GFRP composites are prepared from a GFRP composite square bar of 0.5 in. x 0.5 in. section and that for carbon composites from a CFRP panel of 12 in. x 12 in. x .25 in. From these stocks the samples are machined with the fibers oriented in longitudinal direction. The rectangular samples had a dimension of 1.5in. x 0.5in. x 0.25in. for GFRP composites and 1.5in x 0.375in. x 0.25in. for CFRP composites, which are chosen based on the ASTM standards. The materials used are given in table 3.1. Figure3.1 shows the test samples used.

Material	Lay-up	Dimensions	Testing temperatures
Glass/polyester	Unidirectional (0) pultruded	1.5 in x 0.5 in x 0.25 in	-100ºC, -5ºC, 23ºC, 50ºC and 80ºC
Carbon/epoxy	Unidirectional (0) 50 ply laminate	1.5 in x 0.375 in x 0.25 in	-100ºC, -50ºC, -5ºC, 23ºC and 50ºC

Table 3.1. Materials used for short beam shear testing

GFRP Sample CFRP Sample

Figure 3.1. Test samples

The short beam shear tests are performed in a MTS (model 810 Material Testing System) machine using the Wyoming test fixture (ASTM-D 2344) for three-point bending. The testing machine is shown in figure 3.2 and the Wyoming test fixture in figure 3.3. A schematic of the measurement system is shown in figure 3.4. It consists of a crosshead with a load cell in it to detect the load applied on the sample and a piston, which can move vertically. The piston has a LVDT (linear differential variable transformer), which can sense the piston displacement. The load cell and the LVDT are connected to a controller, which in turn is connected to a CR10 data logging system. The

data logger is again connected to a computer. The tests are performed in an environment chamber, which could be cooled with liquid Nitrogen or heated by a heating coil. Figure 3.5 shows the outside view of the test chamber and figure 3.6 shows the inside view with controller beside, to operate the MTS machine.

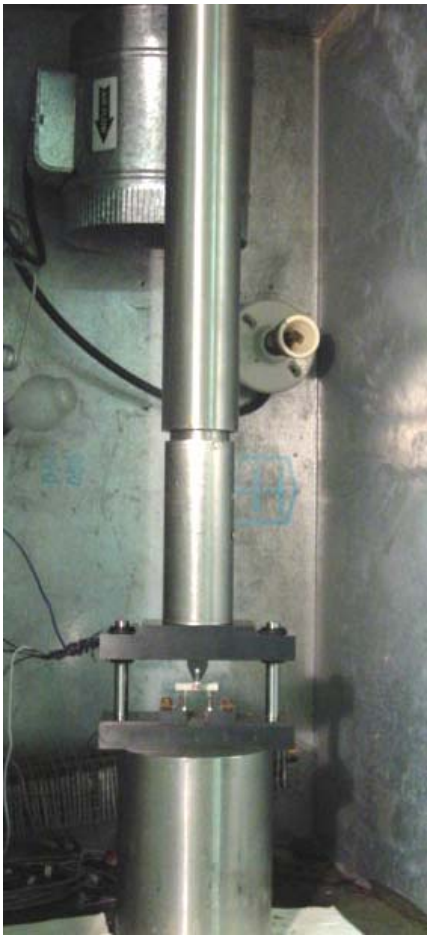

Figure 3.2. MTS machine

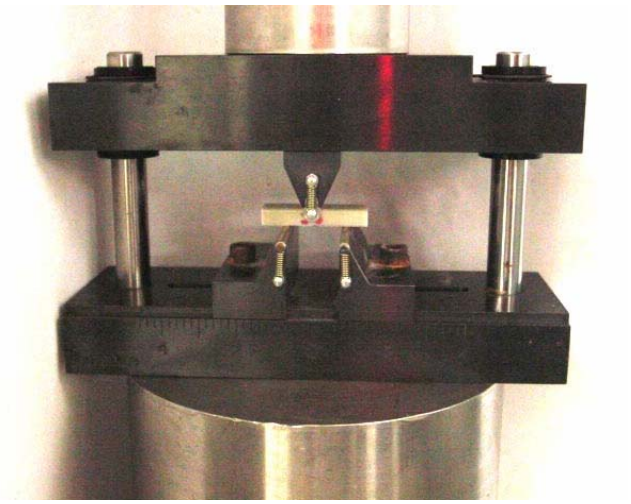

Figure 3.3. Wyoming test fixture

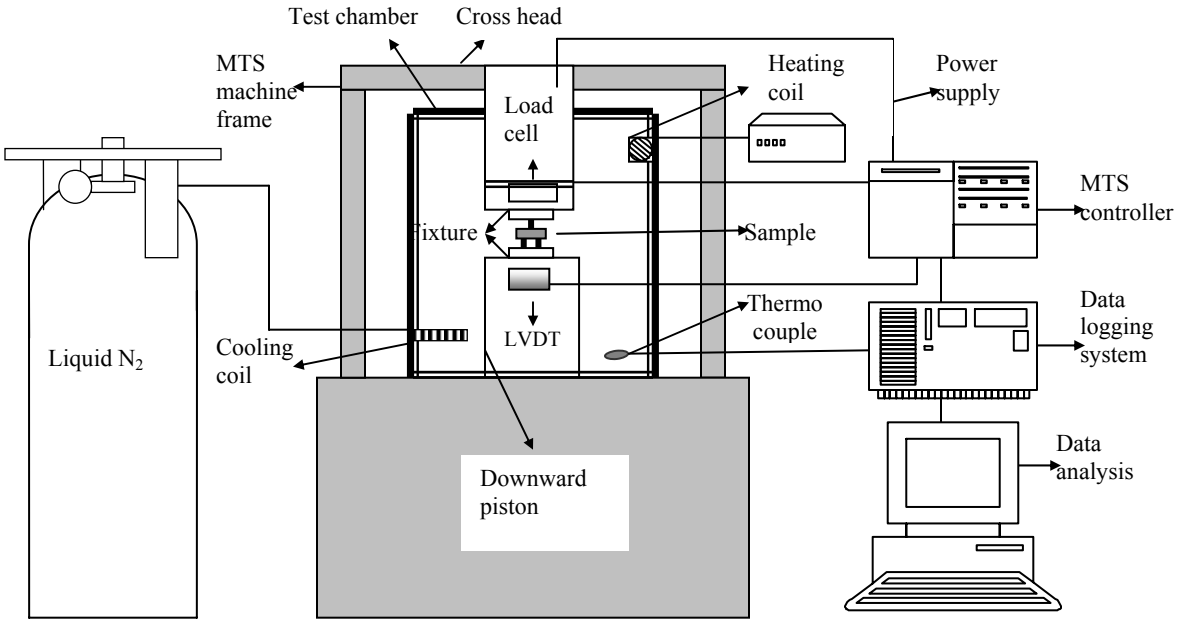

Figure 3.4. Schematic of the short beam shear strength measurement system

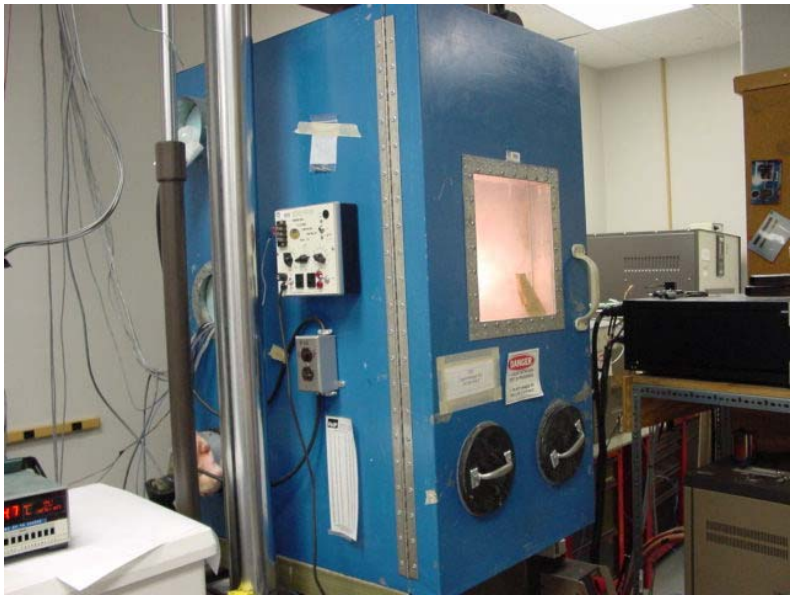

Figure 3.5. Outside view of the test chamber

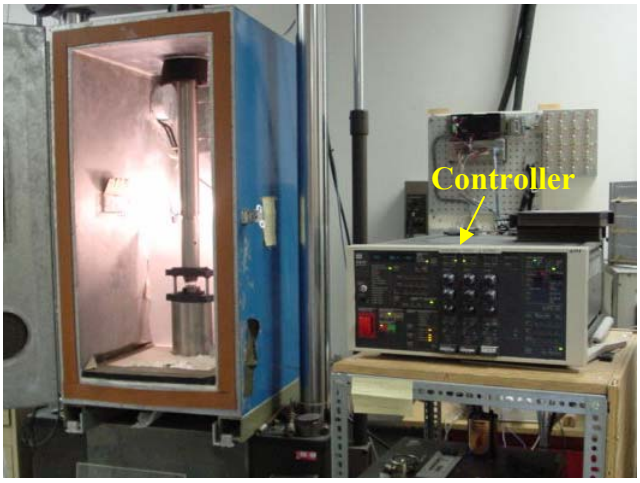

Figure 3.6. Inside view of the chamber with controller to operate the MTS machine

The cooling system involves the supply of liquid nitrogen from the commercially available liquid nitrogen tank through a control valve, which releases the evaporated liquid nitrogen in to the environment chamber. The chamber has tin fins surrounded on a copper rod, which circulates the gas inside the chamber. A feed back loop of temperature sensed by a thermocouple controls the release of liquid nitrogen so that the temperature inside the chamber is maintained steady with in +/- 1ºC. Figure3.7 shows the cooling system. Also the thermocouple is connected to the data logger.

Liquid nitrogen tank

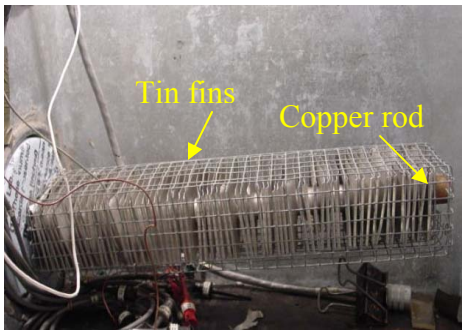

cooling coil in the chamber

Figure 3.7. Cooling system

The chamber could also be heated to a higher temperature by the heating coil mounted inside the test chamber. Figure 3.8 shows the test chamber with the heating coil. Again a feed back loop control using thermocouple controls the temperature of the chamber. The GFRP samples are tested at -100ºC, -5ºC, 23ºC, 50ºC and 80ºC temperatures and CFRP samples at -100ºC, -50ºC, -5ºC, 23ºC and 50ºC temperatures.

Heating coil in the chamber

Temperature recorder

Figure 3.8. Heating system

3.1.2. Testing

For testing, the fixture is attached to the piston and the samples are carefully placed on the test fixture and adjusted to be symmetric with the span of the fixture. Refer figure 3.3. The ASTM standard D2344-95 specifies the length to thickness ratio of 7 and span to thickness ratio of 5 for glass fiber composites but the actual ratios taken were 6 for length to thickness and 3.26 for span to thickness. For carbon fiber composites the ratios specified are 6 for length to thickness and 4 for span to thickness but here the actual ratios taken are 6 for length to thickness and 3.26 for span to thickness. The upper nose of the fixture is made to touch the center of the sample, by means of moving the piston of the servo hydraulic MTS machine in upward direction. Then a quasi-static

compression load is applied on the sample with a constant piston speed of 0.05 in. per minute. Figure 3.9 shows the view of the GFRP samples before and after applying the load and figure 3.10 for CFRP samples. For testing at temperatures other than room temperature the samples are soaked at that temperature for a minimum of 45 minutes. The desired temperature is then attained in the chamber. After the sample reaches a uniform temperature throughout its length, testing is done the similar way as described above. A batch of 5 or 6 samples was tested at each temperature to determine the effect of temperature on the shear strength for each type of sample.

Before After

Figure 3.9. GFRP samples

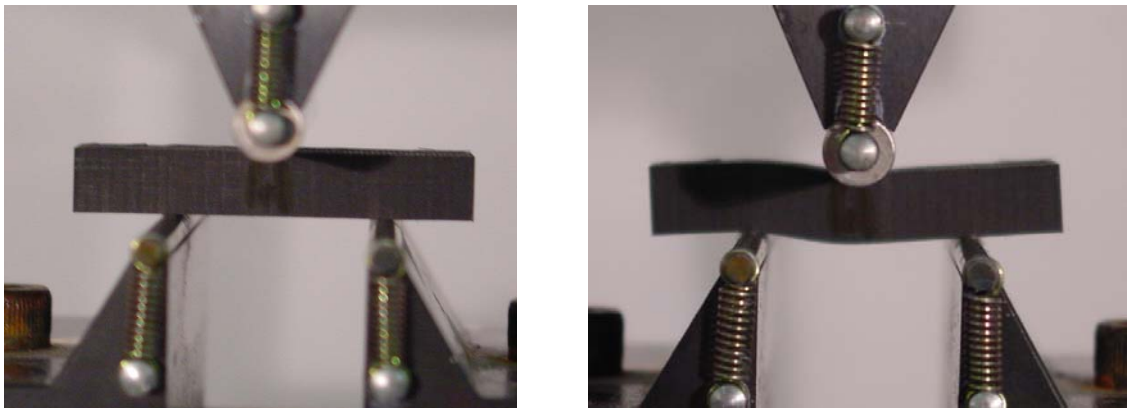

Before After

Figure 3.10. CFRP samples

The force on the sample and the piston displacement are sensed by the load cell and LVDT respectively and transferred to the controller. This data is recorded for every one second by the CR10 data logging system, which is in turn connected to the controller. The piston displacement represents the deflection of the beam because the machine is a rigid system. The data logger also records the temperature inside the chamber by means of the thermocouple. The data logger is connected to a computer and the data is then transferred to an Excel spreadsheet. So the maximum load the sample can take is recorded and the shear strength is calculated using the below equation from ASTM D 2344-95:

$$S_H = \frac{0.75P_B}{bd}$$

where: S_H=shear strength (psi),

P_B=breaking load (lb),

b =width of specimen (in), and

d =thickness of specimen (in)

3.1.3. Results

GFRP composites:

Table 3.2 shows the test results of GFRP samples at -100ºC, -5ºC, 23ºC, 50ºC and 80ºC temperatures. Shear strength (psi) value and the maximum displacement at peak load for different temperatures are shown in the table.

Temp (ºC)	No. of samples	Shear strength S_H (psi)	Deflection at peak load (in)	Standard deviation	% Standard deviation
-100	6	10510.8	0.020	349.7	3.327
-5	6	9014.6	0.021	365.9	4.059
23	6	8309.8	0.022	288.0	3.466
50	6	4926.2	0.031	195.0	3.959
80	6	2721.8	0.051	96.2	3.536

Table 3.2. Test results of GFRP samples at different temperatures

Figure 3.11 shows the variation of shear strength with temperature for GFRP composites, which indicates that the shear strength decreases with increasing temperatures. Figure 3.12 shows the force displacement curves at different temperatures, which show that the load at which the samples fail in shear at lower temperatures is high compared to that at higher temperatures. The sharp peaks at low temperature indicate the brittleness of the composites and the amount of load that can be applied without causing the actual failure is very high. At high temperatures, they tend to become ductile and can sustain only low loads but for a longer deflection.

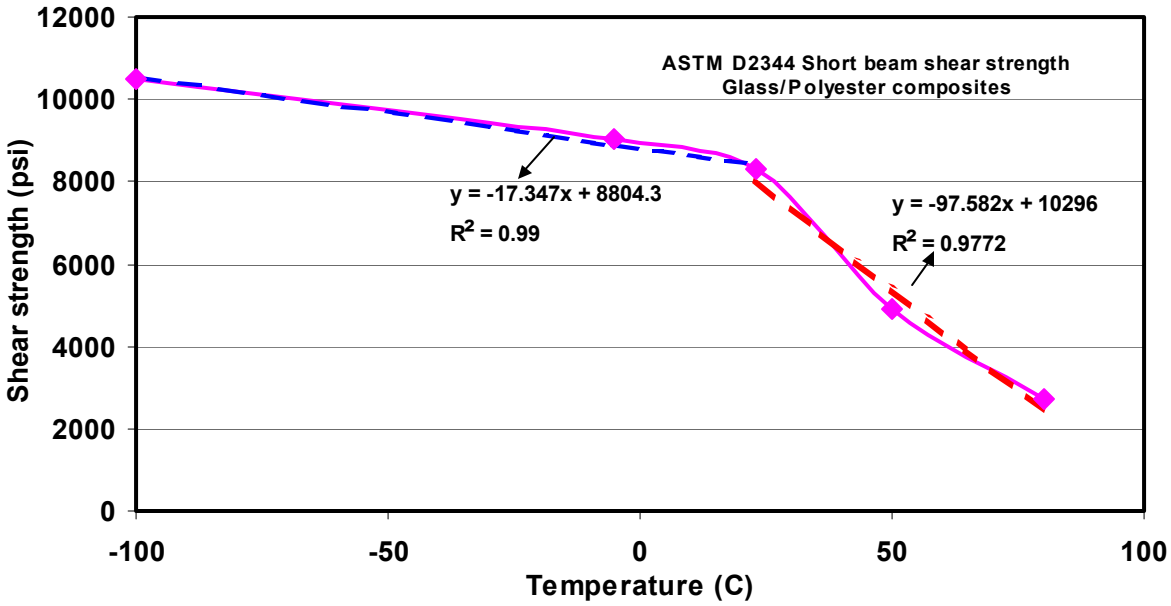

Figure 3.11. Shear strength response with temperature for GFRP composites

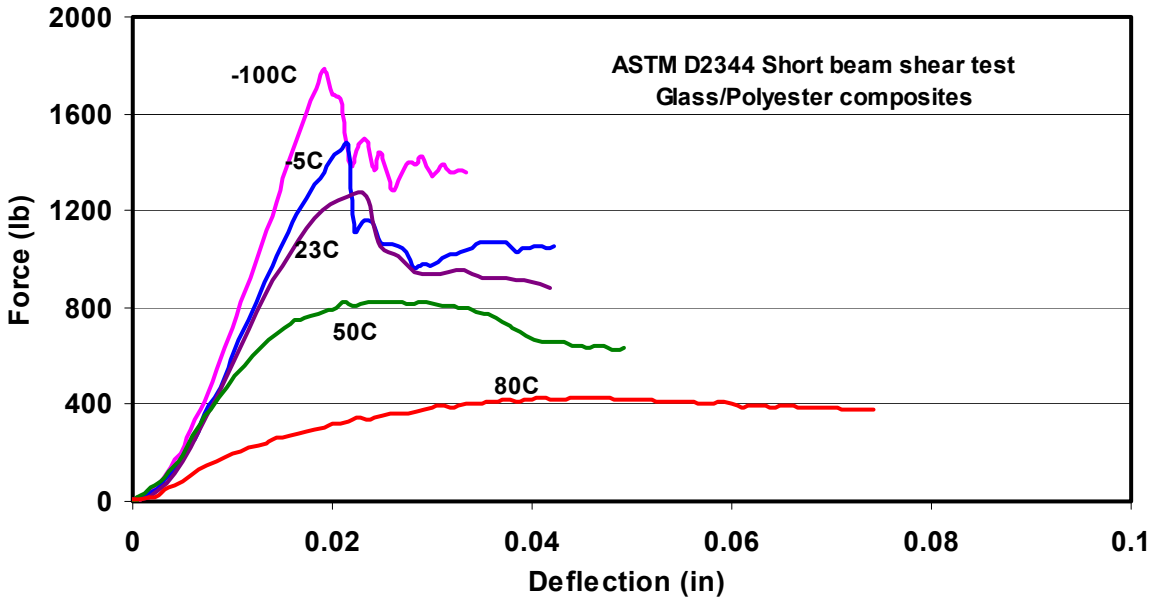

Figure 3.12. Force vs. deflection at different temperatures for GFRP composites

CFRP composites:

Table 3.3 shows the test results of CFRP samples. Figure 3.13 shows the shear strength response of carbon fiber composites to low temperatures.

Temp (°C)	No. of samples	Shear strength S_H (psi)	Deflection at peak load (in)	Standard deviation	% Standard deviation
-100	5	23633	0.046	783.87	3.317
-50	5	17733	0.035	1578.64	8.902
-5	5	14525	0.032	161.06	1.109
23	5	11286	0.029	3247.29	28.774
50	5	11280	0.030	107.41	0.952

Table 3.3. Test results of CFRP samples at different temperatures

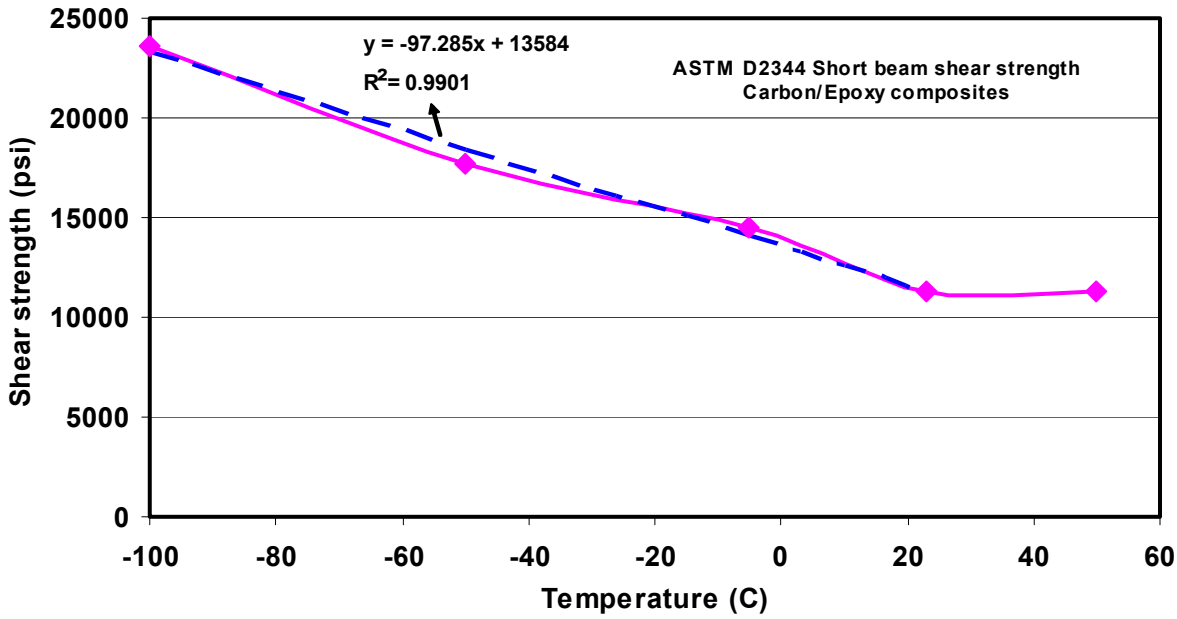

Figure 3.13. Shear strength response with temperature for CFRP composites

Figure 3.14 shows the force displacement curves at different temperatures. The behavior is similar to that of GFRP composites. But at high temperatures, the strength does not degrade as dramatically as in GFRP samples, which is discussed later in chapter

5. They become brittle at lower temperatures and can take more loads. And at high temperatures they become ductile and can bear fewer loads.

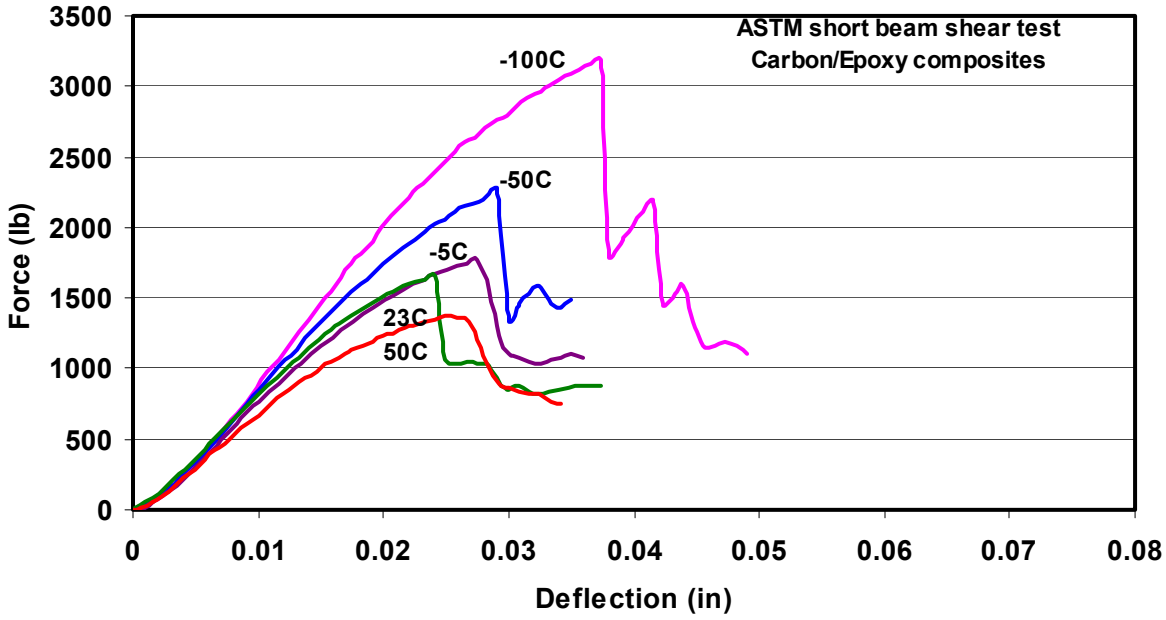

Figure 3.14. Force vs. deflection at different temperatures for CFRP composites

3.2. Acoustic emission testing

Other than the mechanical properties of composites, the damage in composites due to microcrack generation at low temperatures is also studied. It is suspected that the microcracks occurs at cryogenic temperatures as explained in section 2.3. Acoustic emission technique is employed to monitor these microcracks generated due to thermal stresses.

3.2.1. Experimental setup

Material used:

Unidirectional, Carbon/epoxy composites

Lay up: (0) 50 ply laminate

Dimensions: 4in. x 0.75in. x 0.25in.

The test samples were prepared from a CFRP panel of 12in. x 12in. x 0.25in. section. From this stock, the samples were machined with the fibers oriented in longitudinal direction. The rectangular specimens had a dimension of 4in. x 0.75in. x 0.25in. Figure 3.15 shows the test samples used.

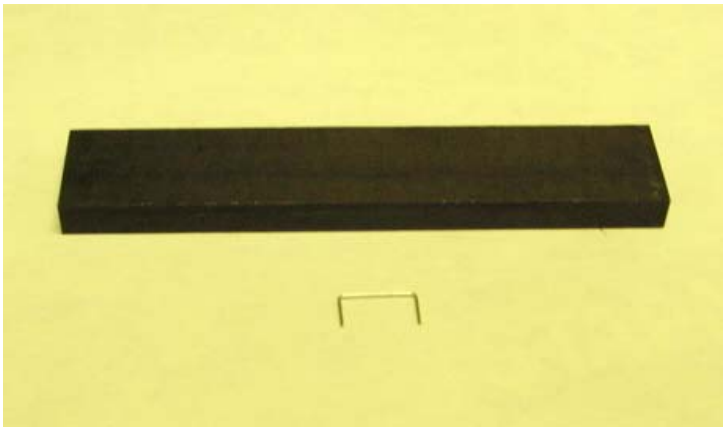

Figure 3.15. CFRP test sample

Figure 3.16 shows a view of the test chamber used. The test chamber is connected to the cooling system, similar to the one used for shear strength experiments in MTS machine chamber. It basically involves the supply of liquid nitrogen from the commercially available liquid nitrogen tank through a control valve, which releases the evaporated liquid nitrogen in to a hollow copper rod inside the environment chamber. The hollow copper rod has tin fins surrounding it, which cool the air and circulate it inside the chamber. A feed back loop of temperature sensed by a thermocouple controls the release of liquid nitrogen so that the temperature inside the chamber is maintained steady with in +/- 1ºC. Refer figure 3.7. Figure 3.17 shows a schematic of the test equipment used.

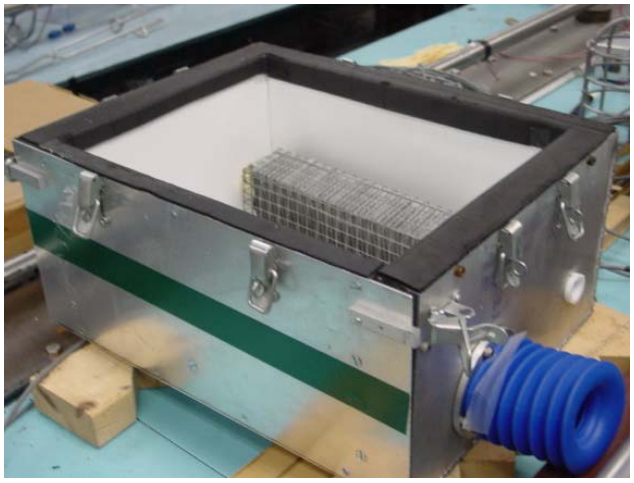

Figure 3.16. Test chamber

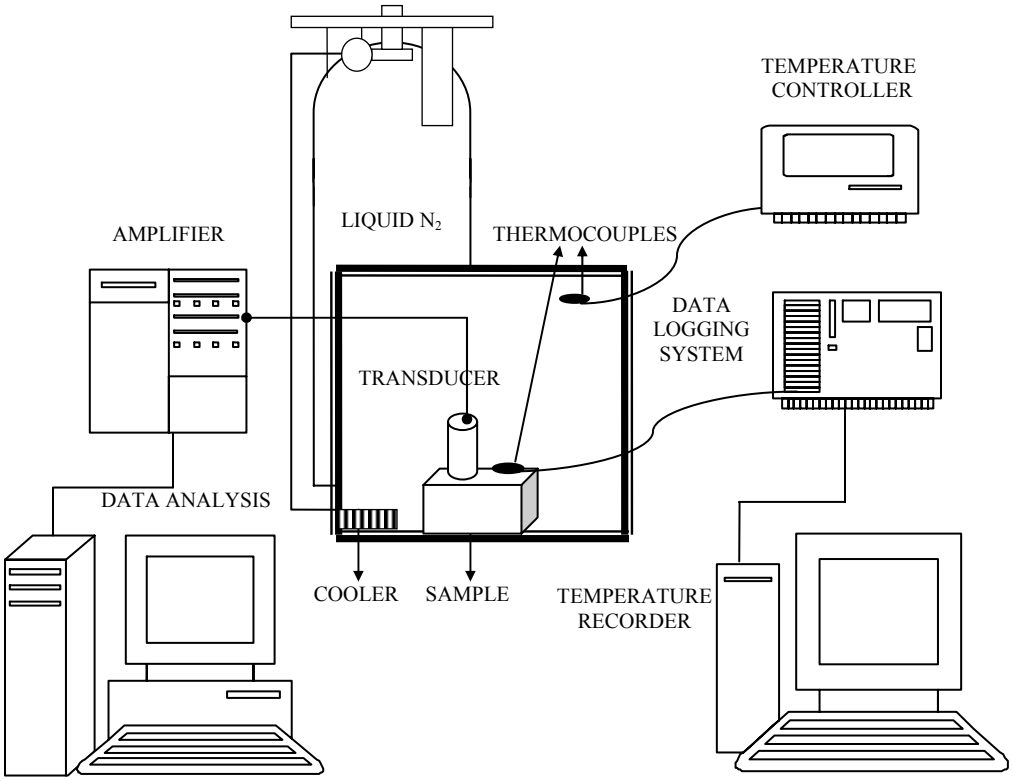

Figure 3.17. Schematic of acoustic emission equipment

A transducer is clamped with the specimen through a coupling medium. Vacuum grease is used as a fluid-coupling medium between the sample and transducer to ensure

the proper transformation of signals from sample to transducer. The transducer used is the generally employed piezoelectric transducer, which converts the surface acceleration in to an electrical signal by means of an amplifier. AE DSP-32/16 PC card or board is connected to the amplifier, which transfers the data to a computer. A thermocouple is clamped with the specimen to note the temperature of sample. The thermocouple is connected to a Campbell Scientific CR10 data logging system, which in turn is connected to another computer.

3.2.2. Testing

For testing, the sample is then placed in a test chamber and clamped with the transducer and thermocouple. Figure 3.18 shows the transducer attached to the sample along with a thermocouple. The chamber door is closed and the whole setup is not disturbed until the end of test.

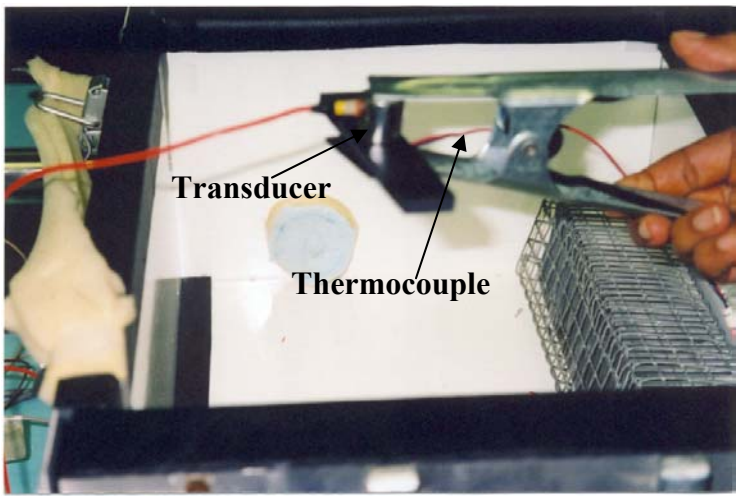

Figure 3.18. Test sample clamped with the transducer and thermocouple

The sample is initially subjected from room temperature to cryogenic temperatures. The selected temperatures are 23, -5, -50, -100, -150°C. The sample is kept at each of these temperatures for 10 minutes, gradually decreasing the temperature. Later

the sample is taken back from –150°C to room temperature. The thermocouple reads the temperature of the specimen and the CR10 data logger records it for every 4 seconds and transfers the data to the computer. As the sample is taken to low temperatures, microcracks are produced and whenever a microcrack occurs, an acoustic event is generated. When a dynamic process such as microcracking occurs in a material, some of the released elastic strain energy can generate stress waves. These stress waves propagate through the material and eventually reach the surface as acoustic pulses. Each pulse above a preset amplitude threshold is termed as an event. The transducer will sense the signals whenever an event occurs (i.e. microcrack generation). The electrical signals are subsequently amplified by means of an amplifier connected to transducer. The PC card connected to the amplifier collects the data of time and accumulated events and sends it to a computer, which uses MISTRAS 2001 software to read the data and then transfer it to an Excel spreadsheet. The MISTRAS software is provided by PHYSICAL ACOUSTICS CORP., NJ. The data of time, events and temperature is recorded throughout. A batch of 4 samples was tested.

3.2.3. Results

Test results are summarized in table 3.4. The results are presented in terms of a cumulative number of counts over the total range of temperature, which indicates the extent of microcrack generation. We see that when the samples are subjected from room temperature to cryogenic temperatures (approximately –150C), the number of events generated is very high (1930 to 3495 events). But when the samples are warmed up to attain room temperature back, the total events generated are very less (33 to 249 events). This clearly indicates that when the composites are subjected to cryogenic temperatures,

the formation of microcracks occur at a very high rate but there are very small number of microcracks formed once the sample is taken back to room temperature. Figures 3.19 thru 3.22 show the plots for accumulated events at a given temperature over a time period of approximately 1600 seconds. Again it is clearly seen that the rate of events increases as the temperature is changed from 23^{o}C to cryogenic temperature (-150C) but from –150ºC to room temperature, the rate of increase of events is very low i.e. the curve of accumulated events is almost flat. This indicates that the number of microcracks produced was high during reducing the temperature and once the lowest temperature is reached, further warming up does not cause any major increase in microcrack formation.

Samples	Temp ºC	Total no. of events on decreasing the temp.	Total no. of events on warming to room temp.
1	-154	1930	33
2	-150	1280	186
3	-150	3789	82
4	-150	3495	249

Table 3.4. Results of acoustic emission testing

Also note from figures 3.19 thru 3.22 that the microcracks do not often occur immediately as the temperature is reduced but usually there is a time lag. For example in figure 3.21 the temperature was reduced in many steps as 23, 0, -5, -20, -50, -100 and -150C keeping the sample to cool at these temperatures for about 10 min but most of the microcracks occurred around 2000 seconds of time when the temperature was changed from 0C to –50C.

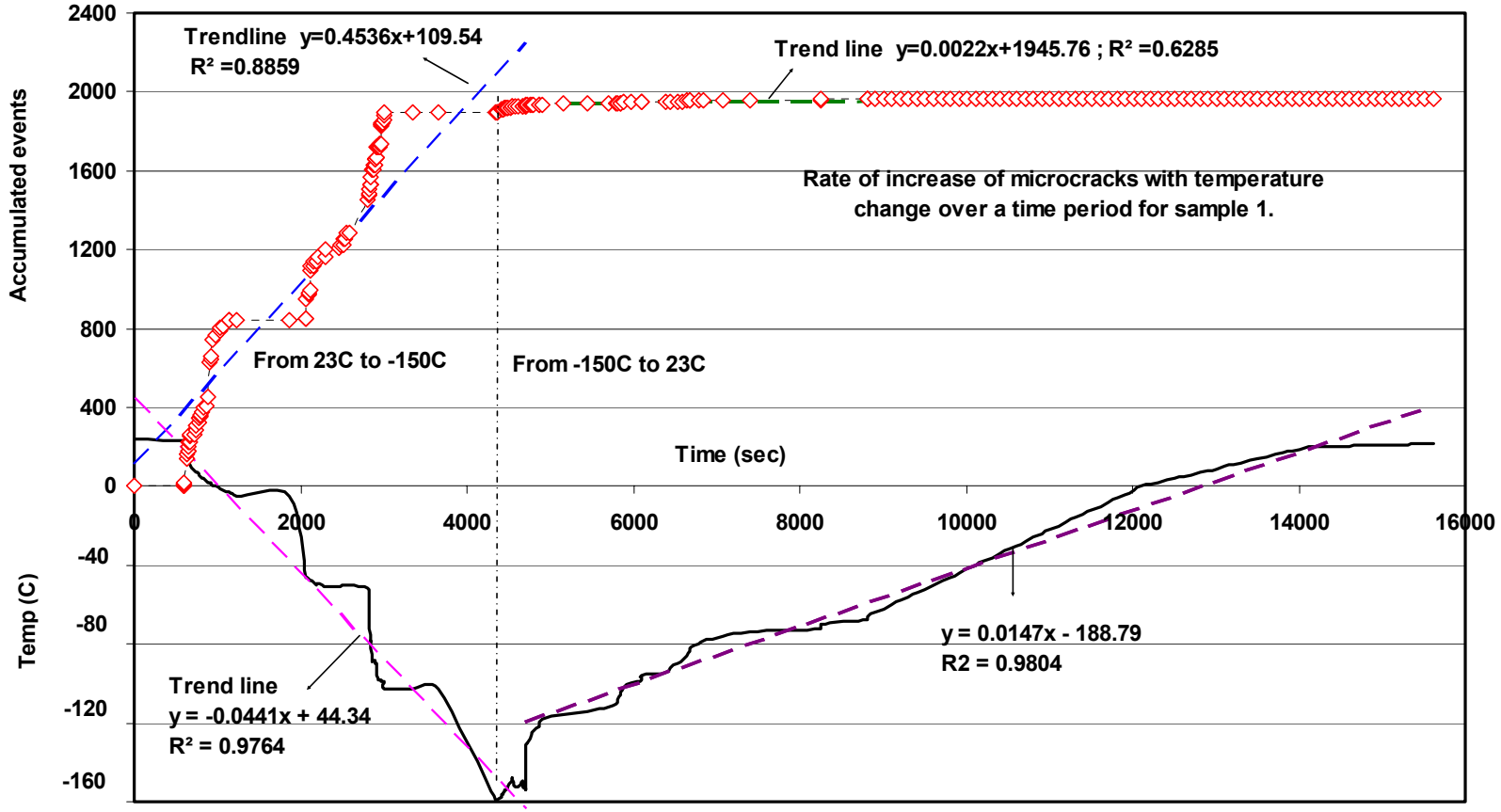

Figure 3.19. Change of acoustic events with temperature

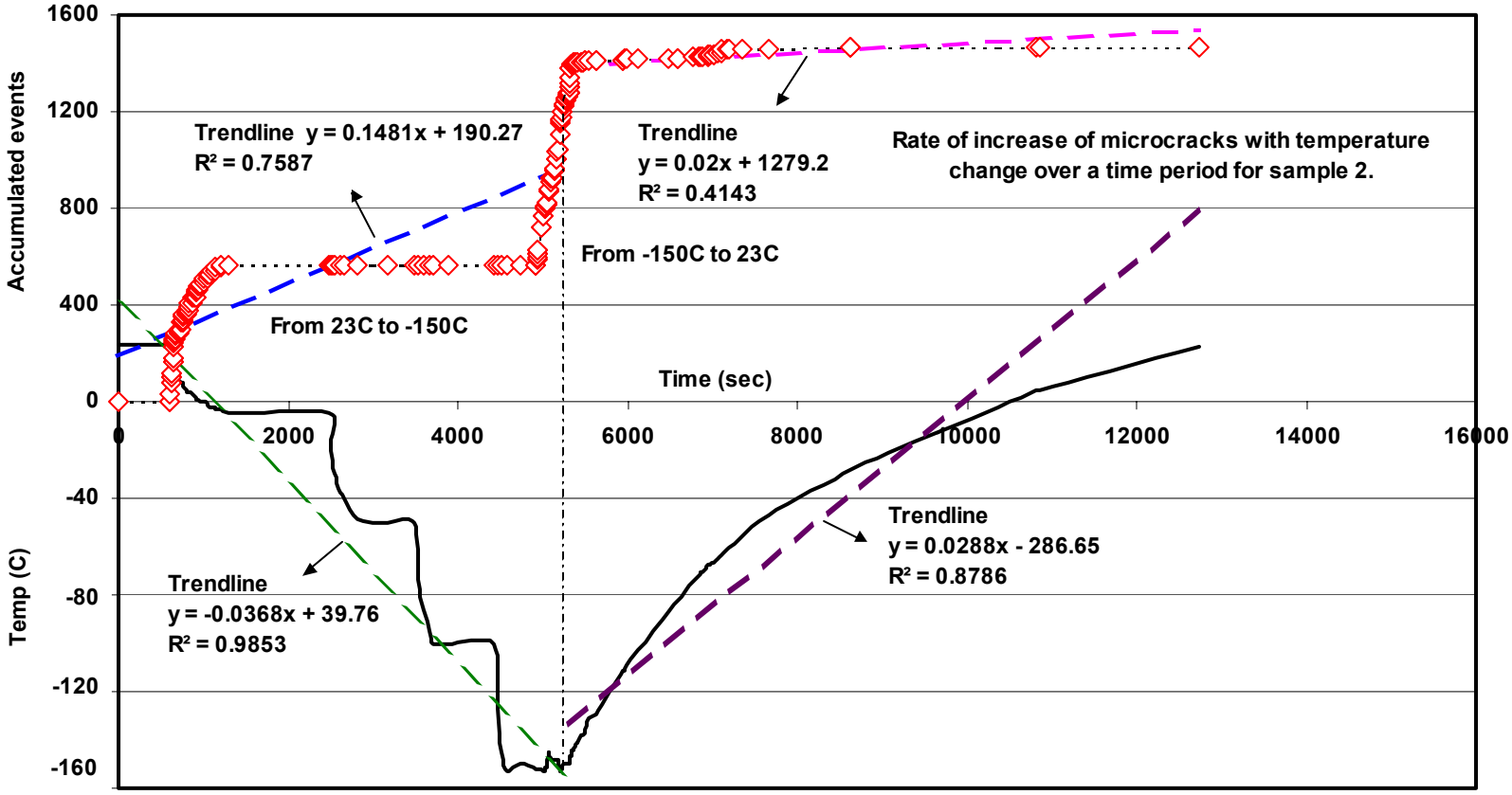

Figure 3.20. Change of acoustic events with temperature

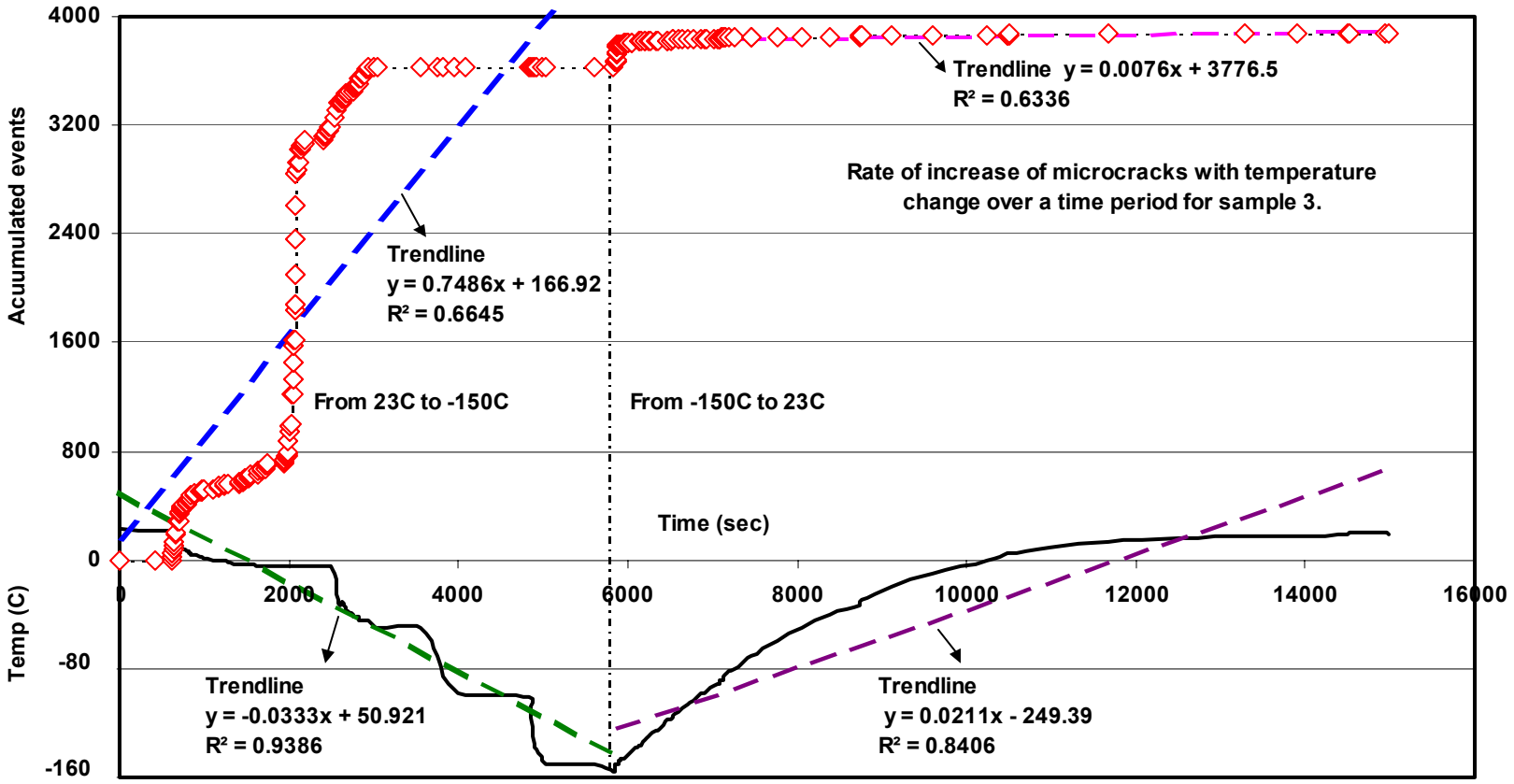

Figure 3.21. Change of acoustic events with temperature

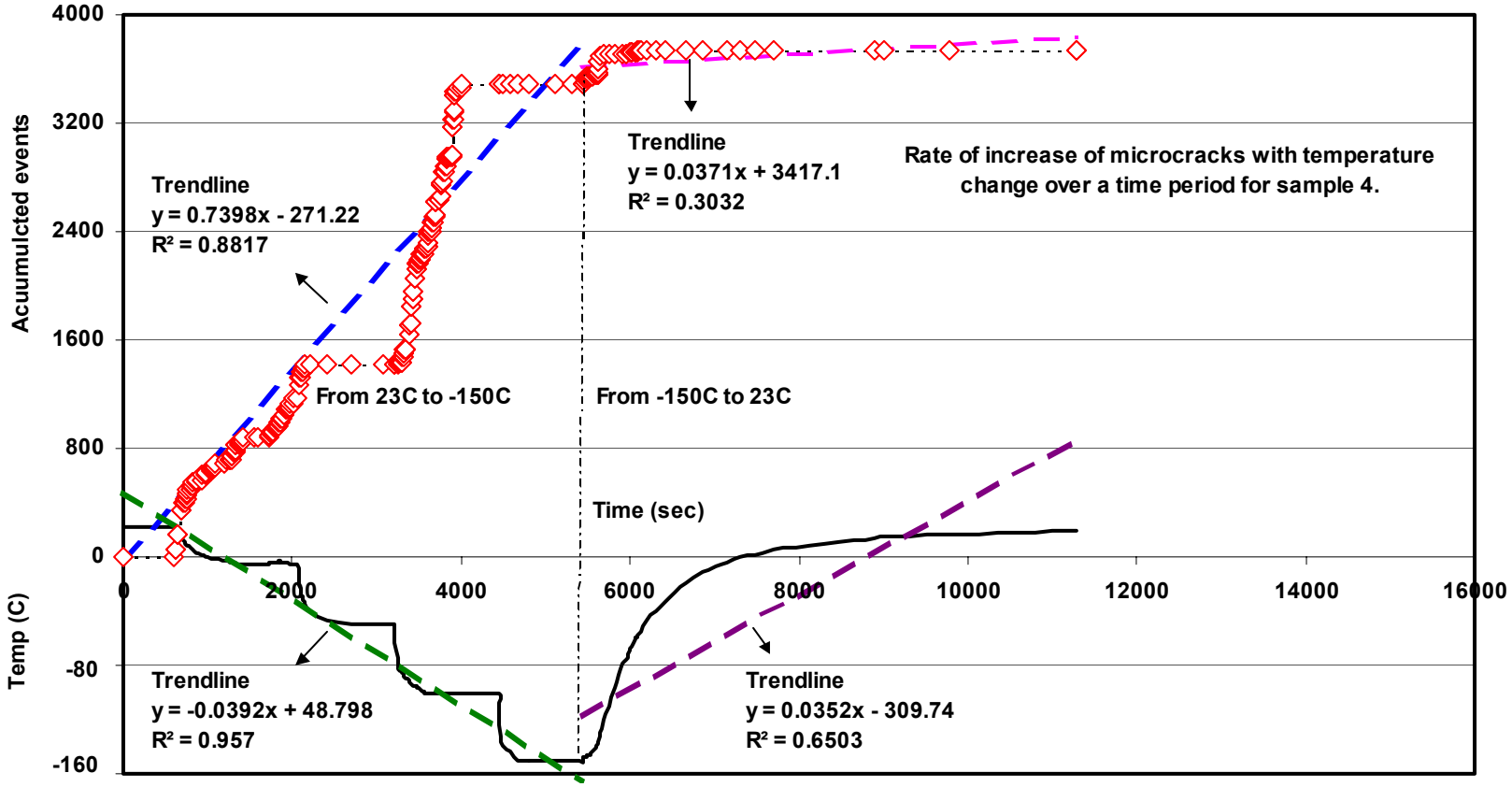

Figure 3.22. Change of acoustic events with temperature

4. Design of permeability equipment

In previous chapter it is shown by experiments that not only the mechanical properties of composites do change by reducing the temperatures to extremely low levels but they do develop large number of microcracks as well. Concerns are raised whether such microcracks can increase the permeability of composites or not. For this purpose it is essential to perform experiments to find out the permeability of composite samples when subjected to cryogenic temperatures. In this chapter it is described that how a permeability apparatus can be designed and built to perform such experiments. It is based on allowing the test gas fluid to permeate through the samples and noting down the change of pressure. A rapid change of pressure would indicate a higher permeability of the material.

4.1. Description of equipment:

In this section equipment is designed to measure the permeability of various composite materials to different fluids or gases.

The equipment shown in figure 4.1 consists of a storage chamber made of aluminum in cylindrical shape, which has threads on both the ends. On one end is a fixture ‘F1’ attached with an inlet connected to a tank, which supplies the test gas (nitrogen for testing at liquid nitrogen temperature) to flow in to the chamber. At the other end a fixture ’F2’ is attached which holds the sample in it. The fixture ‘F2’ is shown in figure 4.2. An exhaust pipe to allow the gas leaking out of the sample to escape

to atmosphere is connected to this fixture with an adaptor and a swivel nut. An outlet pipe with a valve is also connected to the chamber. The chamber is also equipped with a precision pressure transducer. One thermocouple is placed inside the chamber and one outside the chamber, which are connected to the temperature recorder. Other than room temperature if the testing is to be done at low temperatures then the whole equipment is immersed in the cryogenic liquid contained in a dewar (doubled walled vessel with a high vacuum in the space between the walls) as shown in figure 4.3.

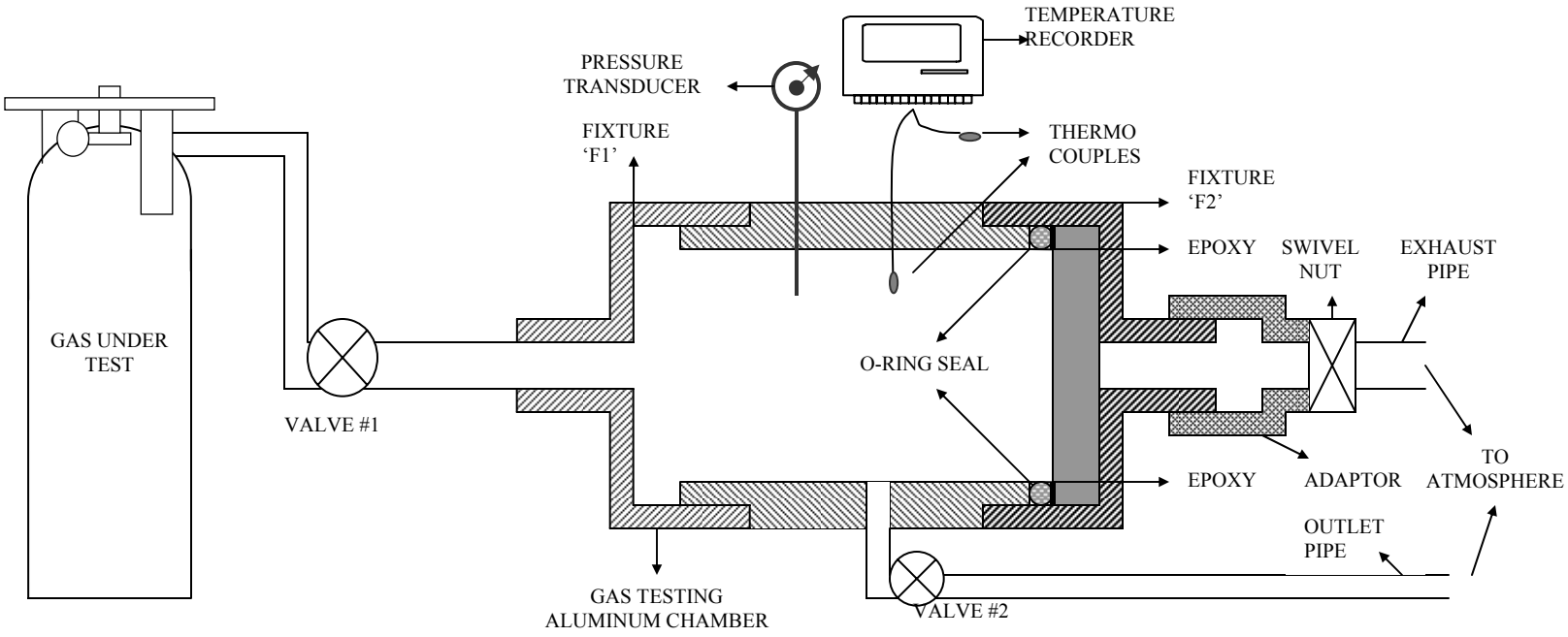

Figure 4.1. Design of the permeability equipment

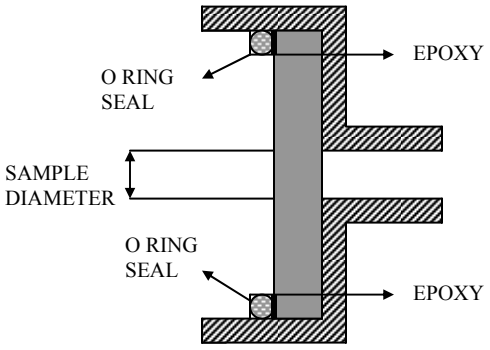

Figure 4.2. Fixture 'F2'

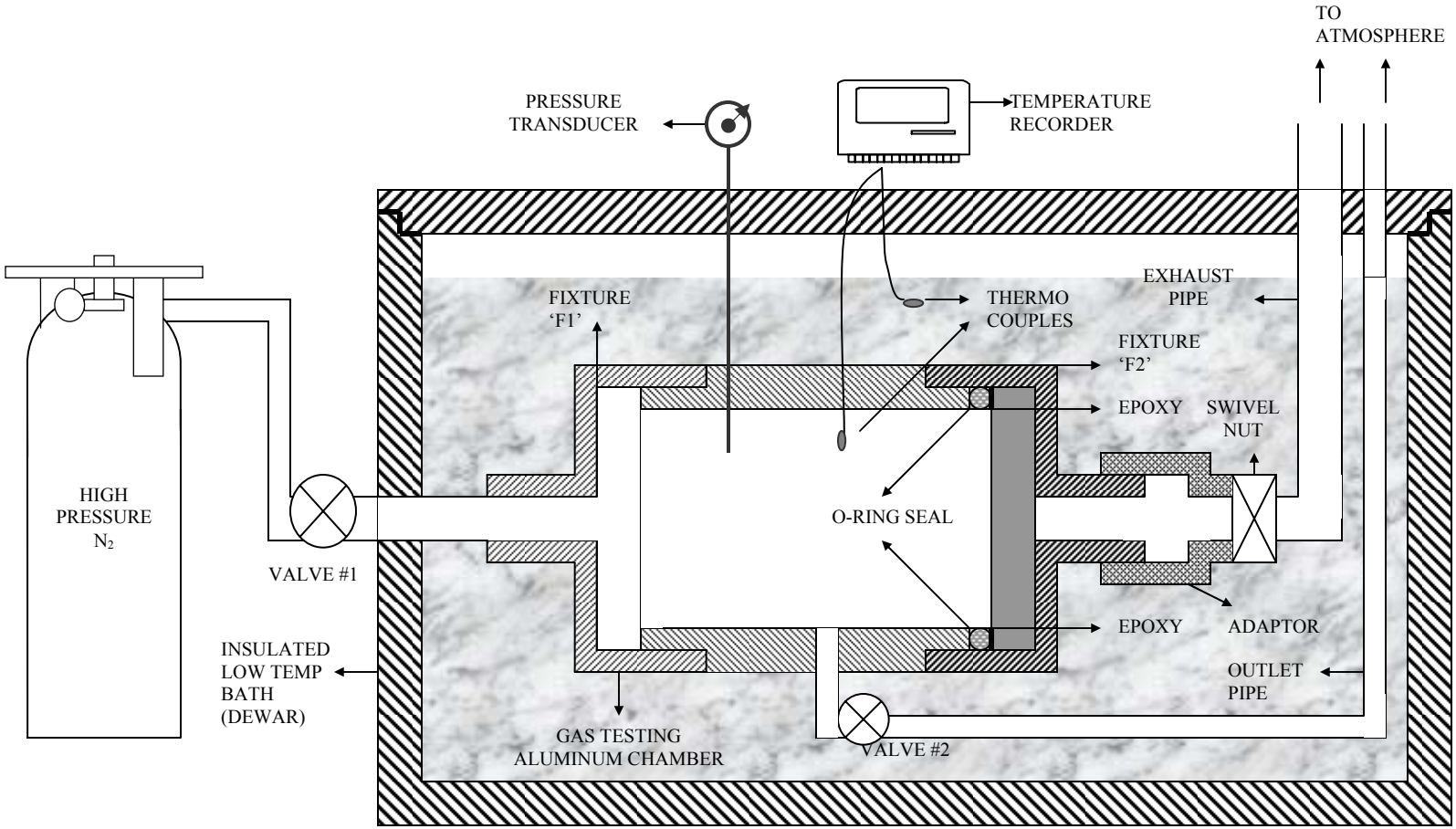

Figure 4.3. Permeability equipment immersed in a low temperature bath

4.2. Working procedure:

Initially a composite sample of circular shape and desired thickness is chosen and the area, 'A' of the sample across which the gas flows and the thickness, 'h' in the direction in which the gas flows is measured. Before testing for permeability, the sample is exposed to low temperatures (say, -10C, -20C, or –100C, -150C) for generating the microcracks. The extent of microcracks generated will depend on the lowest temperature to which it is subjected. The volume, 'V' of the storage chamber with the sample in it is measured. To test, the sample is first placed in the fixture and epoxied in position as shown in figure 4.2. For each sample separate fixture is made. The fixture is then fixed tightly on the threads along the circumference of the storage chamber. Care has to be taken that the fixing of the sample is airtight for which O-ring seal can be used. O-rings, which are suitable for cryogenic temperatures such as silicon O-rings should be used when the low temperature tests are performed. The chamber is then connected to the cylinder of the test gas through a valving system. Now the gas is allowed to flow in to the chamber by opening the valve#1. Also the valve#2 is kept open. As the gas entering is at high pressure, the air in the storage chamber is pushed out through the outlet pipe. After the air has been removed and the chamber is flooded with gas under test, valve#2 is closed. Temperature of the chamber is recorded by the thermocouple. After valve#2 is closed pressure inside the chamber is controlled by manipulating valve#1 which controls the flow of high pressure gas under test and pressure transducer will record the pressure. Also temperature may change as a result of the temperature of incoming gas. Both the pressure and temperature transducers are connected to a data acquisition system. When the desired pressure P_1 is attained, valve #1 is closed tightly stopping the further flow of

gas in to the chamber. For room temperature test allow the temperature with in the chamber to stabilize to ambient temperature. Incase of low temperature testing, it would be necessary to put the chamber inside a good insulated chilled nitrogen cooled temperature bath. For all tests, sufficient time should be allowed for the chamber temperature to attain bath temperature.

To start the test, timer is started and the time and pressure inside the chamber is noted through out the test at regular intervals. The gas in storage chamber is at high pressure than outside pressure and will therefore permeate through the sample. Since the equipment is completely sealed, any fall in pressure will indicate gas leakage. This leakage of gas would be attributed to the microcracks in the sample. As the gas leaks through the sample to atmosphere, pressure in the chamber starts decreasing. The quantity of gas leaking, 'Q' over a period of time 't' has to be measured, which is explained further below. Hence the new pressure, P_1' and the time, t, to attain this pressure can be noted at any point.

The permeability measured here is according to Cogswell

(1992). From the Darcy's law referred in section 2.4, the permeability coefficient D, is rewritten as:

$$D = \frac{\eta v h}{P'_1 - P_2} \quad \text{(units: in}^2\text{)} \quad \text{---------- (1)}$$

where η= viscosity of the gas (lbf s/in^2)

v= mean velocity of the gas (in/s)

h= thickness of the sample in the direction of gas flow (in)

$P_1'-P_2$= pressure difference measured across the sample (psi)

Note: As the gas is leaking to the atmosphere throughout the test, the pressure P_2 is taken as $P_2 \approx 14.5$psi (STP). For expressing permeability in other units, see section 2.4.

The mean velocity is defined as $v = \frac{Q}{At}$ ---------- (2)

where Q= quantity of gas leakage (cubic in.)

A= area of the sample measured across the flow (in^2)

t= total time taken for the gas to cross the sample thickness (sec)

The quantity of flow, 'Q' is measured using the Boyle's law, which gives a simple relationship between the pressure and volume of a gas in a container at constant temperature. If P_1 = Initial pressure in the storage chamber (psi)

V = Initial volume of gas in the storage chamber at initial pressure (cu. in.)

P_1'= Final pressure in the storage chamber (psi)

Then after some time as the gas leaks the pressure decreases to P1', although the gas occupies the same volume, V, as that of the chamber. We need to determine what would be the volume of the gas remaining in the chamber if it was subjected to the initial pressure P_1.

V'= Final volume of gas in the storage chamber at initial pressure (cu. in.)

Then according to Boyle's law

$$P_1 V' = P_1' V$$

$$V' = \frac{P_1' V}{P_1} \qquad \text{---------- (3)}$$

and

$$Q = V - V' \qquad \text{---------- (4)}$$

As P_1 and V are measured initially before starting the experiment and P_1' can always be measured at any point of time and the constant temperature conditions are maintained throughout, the final volume V' can be calculated using eq.(3). Also the quantity of flow of gas Q can be calculated by substituting V' from eq.(3) into eq.(4).

$$Q = V - \frac{P_1' V}{P_1}$$

$$Q = \frac{V(P_1 - P_1')}{P_1} \qquad \text{---------- (5)}$$

Now substituting the Q, area (A) of sample and time (t) values for mean velocity, v can be found out according to eq.(2). Substituting 'Q' from eq.(5) in to eq.(2)

$$v = \frac{V(P_1 - P_1')}{P_1 A t} \qquad \text{---------- (6)}$$

Knowing the viscosity (η) of gas, thickness (h), of the sample and pressure P1' at any point, the permeability (D) can be calculated as described above in eq.(1). Substituting 'v' from eq.(6) into eq.(1)

$$D = \frac{\eta V (P_1 - P_1') h}{P_1 A t (P_1' - P_2)} \qquad \text{---------- (7)}$$

4.3. Analysis

Permeability is a material constant and same material with different number of microcracks will have different values of permeability. Using eq.(7) analysis has been made to find the effect of change of pressure (across the sample) on the permeability of

the material. The graph that indicates the change in permeability value with pressure change in the chamber is plotted taking assumed values:

Sample thickness h=1 in.

Sample radius=2 in.

Sample area A=12.56 sq.in.

Chamber radius=4 in.

Chamber volume V=175.8 cu.in. (chamber volume considered after deducting the sample volume)

Viscosity of the gas η (Nitrogen gas at STP)=$2.41*10^{-9}$ lbf s/in^2

Initial pressure in the chamber at the start of the test P_1=1000 psi

Atmospheric pressure P_2=14.5 psi

The pressure decrease in chamber is considered for every 1 second. The new pressure in the chamber P_1' is assumed to decrease 40 psi for every 1 sec and the permeability is calculated from the eq. (7). We see that the change of permeability with pressure change is nonlinear from the graph in figure 4.4.

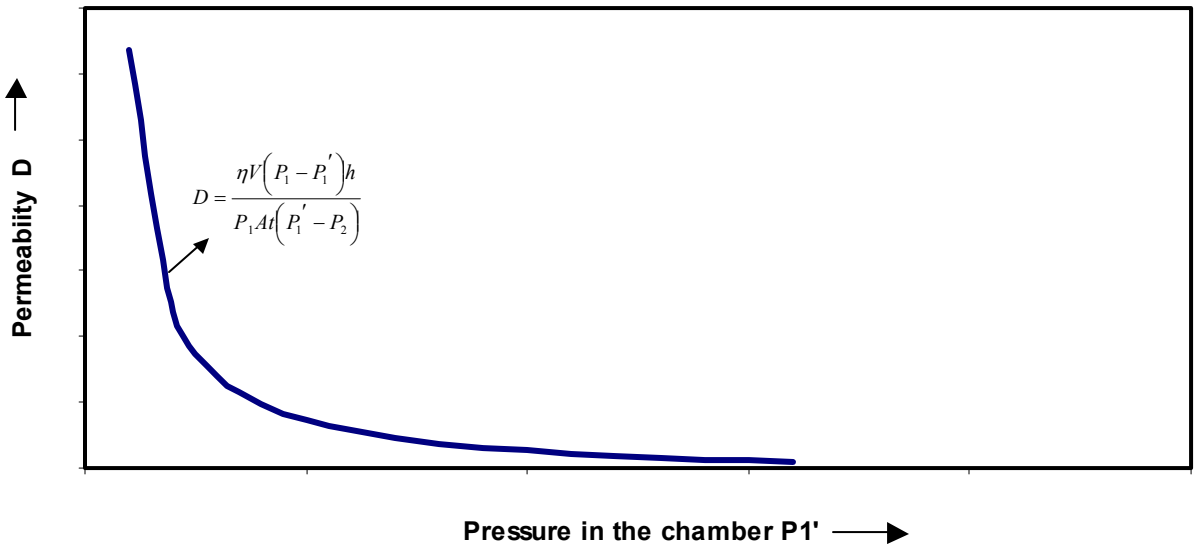

Figure 4.4. Variation of permeability with change in the chamber pressure

If the pressure in the chamber remains high after a specific period of time from the start of the test, permeability is low. This means that if the composite is less porous, the pressure in the chamber remains high for a long time and the permeability of the material is low. Similarly if the material has many cracks or if it is more porous, the pressure in the chamber decreases at a high rate and the permeability of the material is high. So this system can be used to measure the permeability of composites.

It can also be explained in other way that depending on the materials permeability value, the pressure in the chamber decreases at different rates. So from a known permeability value of a material, the pressure decrease rate in the chamber can be obtained. From equation (7) we get that,

$$P_1' = \frac{P_1\left(\eta h V + DAtP_2\right)}{DAtP_1 + \eta h V} \qquad \text{---------- (8)}$$

Again from the values mentioned above for figure 4.4, the pressure change with time is estimated for a permeability value of $3.42*10^{-14}$ in^2. The graph of pressure change with time that represents the equation (8) is given in figure 4.5.

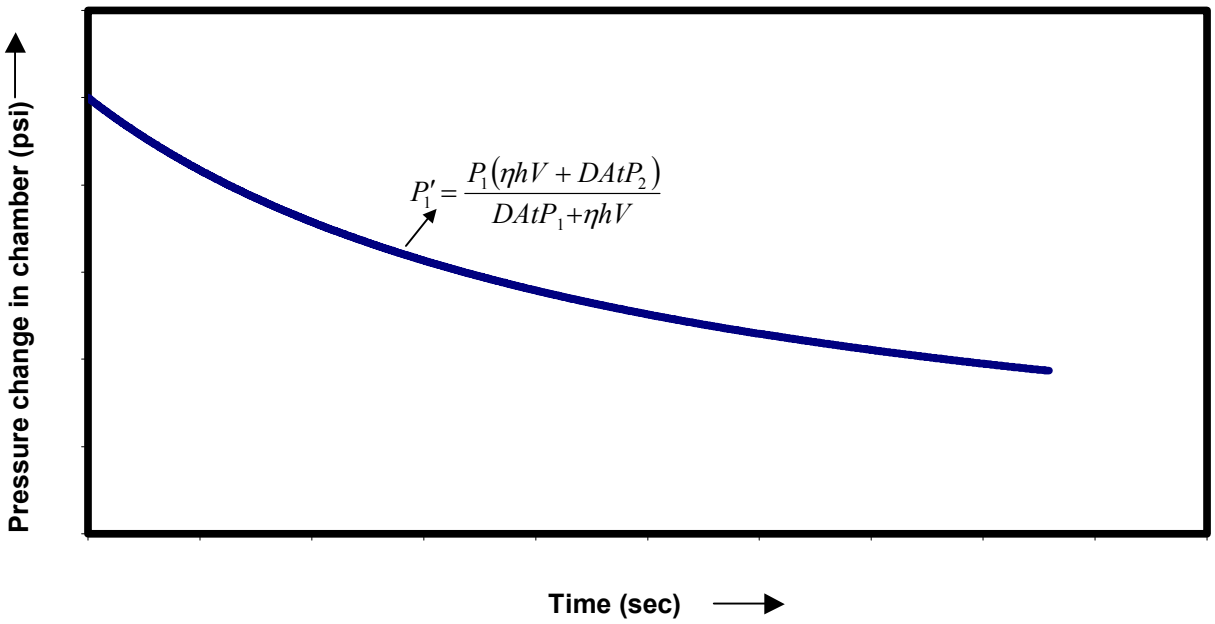

Figure 4.5. Pressure decrease in chamber with time

We see that the pressure decrease in chamber may not be linear with increase in time. It shows that for a known permeability value, the time required for the pressure to decrease to certain value can be estimated.

If the viscosity effect on permeability is considered then the Eq. (7) may vary. Viscosity is the measurement of a fluid's resistance to flow. Viscosity of a gas/fluid changes with temperature but here in this equipment since the temperature is kept constant it does not affect. But if the change of viscosity with pressure is considered then viscosity is a function of the pressure in the chamber. And viscosity ηcan be given as:

$\eta = k + cP_1'$ (Reference: Magna projects and instruments)

where k and c are constants, which vary for each gas/fluid. P_1' is the pressure inside the chamber. Also the permeability eq. (7) changes as

$$D = \frac{\left(k + cP_1'\right)V\left(P_1 - P_1'\right)h}{P_1 At\left(P_1' - P_2\right)}$$

Also eq.(8) changes to

$$P_1'^2 chV + P_1'\left(DAtP_1 + khV - chVP_1\right) = P_1\left(khV + DAtP_2\right)$$

The relationship above for permeability and pressure may also deviate from the curve depending on the change of viscosity with pressure, which varies for each gas.

5. Discussions

This chapter discusses the results presented in chapter 3.

5.1 Mechanical properties - shear strength:

The shear strength of GFRP composites is high at cryogenic temperatures and low at higher temperatures. Possibly the higher temperatures softened the matrix of the composite. From figure 3.11 it was observed that from 23ºC to 80ºC shear strength decreases drastically and from 23ºC to -100ºC shear strength increases but at a lower rate. The increase in shear strength with temperature reduction for GFRP composites between cryogenic temperatures (-100ºC) and room temperature (23ºC) can be modeled by the following equation:

$S_H = -17.347\ T + 8804.3$

where

S_H = Shear strength (psi)

T = Temperature (°C)

And the shear strength change with temperature between 23C and 80C can be given by the following equation:

$S_H = -97.582\ T + 10296$

where S_H and T are same as explained above.

For CFRP samples also shear strength increases with reducing temperatures as seen in figure 3.13 but the increase is drastic from 23ºC to -100ºC and from 23ºC to 50ºC no increase or decrease in shear strength was obtained. The variation of shear strength with temperature at cryogenic temperature for CFRP composites from -100ºC to 23ºC range can be modeled by the following equation:

$S_H = -97.285\ T + 13584$

where S_H and T are same as explained before.

Like GFRP composites, we expected a reduction of shear strength at higher temperatures for CFRP composites. Whether this trend would be true or not would have been found if some more high temperature tests were performed. Since the major mechanism of shear strength decrease is the degradation of the matrix, it is also possible that the epoxy in CFRP does not degrade as rapidly as polyester of GFRP with rise of temperature. So the decrease rate of shear strength from 23ºC to 50ºC for CFRP is only marginal from 11286 psi to 11280 psi.

Comparing the shear strength of CFRP and GFRP, we observe that the shear strength of CFRP is more than that of the GFRP composites. The shear strength value of CFRP samples (23633 psi at -100ºC) is almost double that of GFRP samples (10510 psi at -100ºC) at low temperatures. Also at 50ºC the value is double (11280 psi for CFRP and 4926 psi for GFRP). So we can say that the carbon/epoxy composites are much stronger than glass/polyester composites. It can also be said that the polymer polyester is more softened than epoxy at higher temperatures.

On the whole we can say that the effect of cryogenic temperatures on composite materials is not to deteriorate the mechanical properties but in fact the shear strength increases as temperature decreases.

The strain of the samples is also calculated based on the deflection, which is explained further. Reference: Motto, (1990)

For a simply supported beam with the load at the center, the deflection, y is given by: $y = \frac{PL^3}{48EI}$ ----------(1)

where P= load applied

L= length of span

E=young's modulus

I=moment of inertia

and the stress, σ is given by:

$\sigma = \frac{Mc}{I}$ ---------- (2)

where M=bending moment

c=half of the sample thickness

also strain, $\varepsilon = \frac{\sigma}{E}$ ---------- (3)

from equations (1), (2) and (3) we get $\varepsilon = \frac{24yc}{L^2}$

From the graphs plotted for strain and force in figure 5.1, we see that GFRP samples are breaking at lower strain than that of CFRP samples at all temperatures, which means that the GFRP composites are more brittle than CFRP composites.

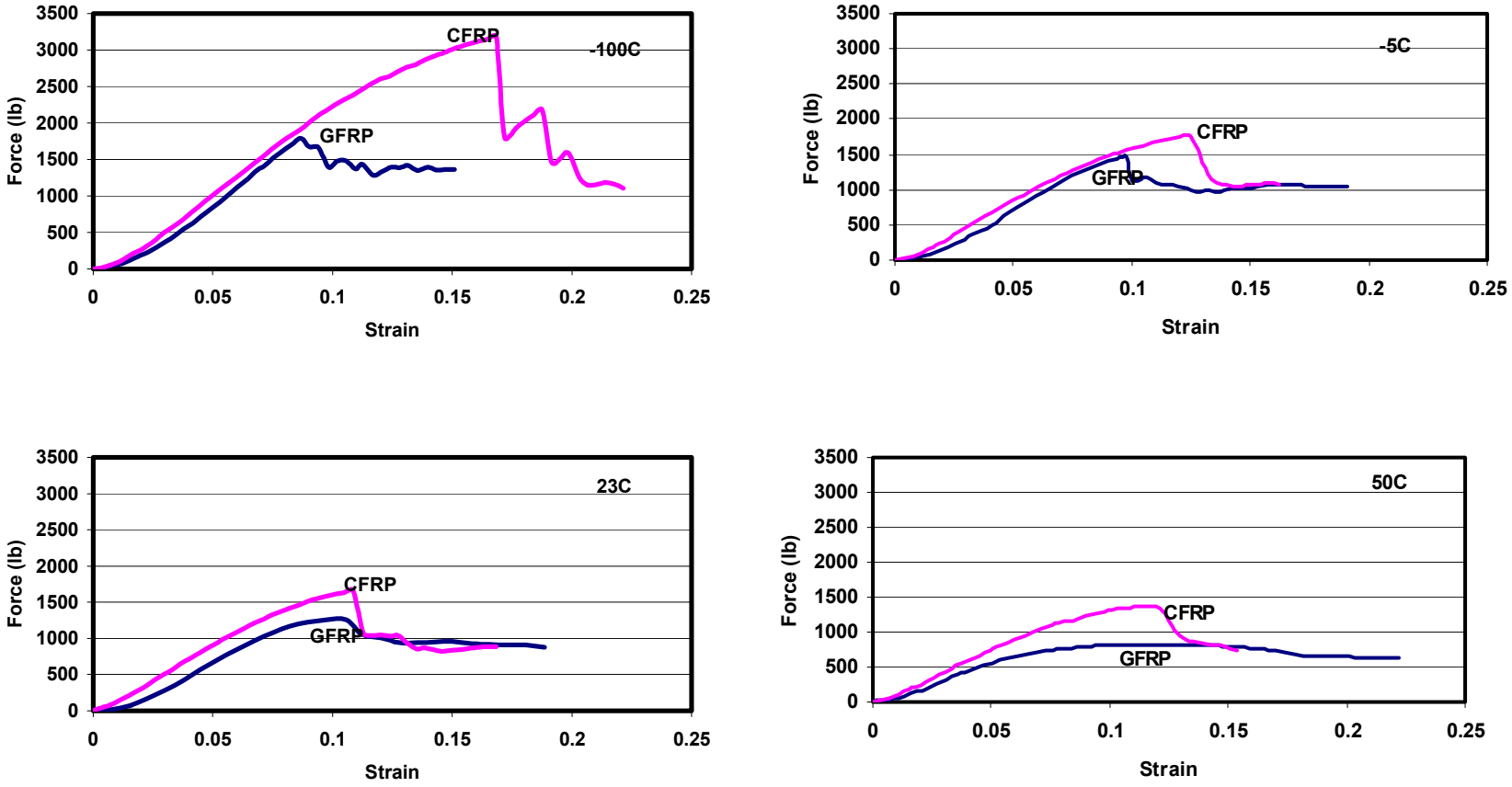

Figure 5.1. Force and strain curves for GFRP and CFRP samples at different temperatures

5.2. Microcracks:

But the other aspect of low temperatures is the damage in composites due to microcrack generation. In fiber reinforced polymer matrix composites, the coefficient of thermal expansion of the matrix and fibers is usually different and in most of the cases matrix has higher order of magnitude than that of the fibers. Contraction of the matrix is resisted by relatively stiff fibers through fiber-matrix interface bonding, setting up residual stresses within the material microstructure and residual stresses may be sufficiently large to cause microcracking with in the matrix and matrix-fiber interfaces. Composite material damage usually begins with the formation of microscopic cracks in the matrix or at the matrix-fiber interface. So to ensure whether the microcracks were actually generated at cryogenic temperatures, Acoustic Emission method was employed. Every event generated is due to a microcrack formed which is due to the thermal stresses setup.

It was observed from figures 3.19 thru 3.22 that when the composites are subjected to cryogenic temperatures, the formation of microcracks occurs at a very high rate but there are almost no or very less microcracks formed when the sample is taken back to room temperature. An index ϕ is defined as the ratio of rate of microcrack growth (dM/dt) to the rate of temperature change (dT/dt) over a time period 't'.

$$\phi = \frac{dM/dt}{dT/dt}$$

The ϕ values are obtained from the trend lines of the graphs in the figures 3.19 thru 3.22, which are tabulated in the table 5.1.

Test No.	Decreasing temperatures				Increasing temperatures			
	dM/dt	dT/dt	ø	ø average	dM/dt	dT/dt	ø	ø average
Test1	0.4536	0.0441	10.2857	13.8730	0.0022	0.0147	0.1497	0.5646
Test2	0.1418	0.0368	3.8533		0.0200	0.0288	0.6944	
Test3	0.7486	0.0333	22.4805		0.0076	0.0211	0.3602	
Test4	0.7398	0.0392	18.8724		0.0371	0.0352	1.0540	

Table 5.1. *ø* values for increasing and decreasing temperatures

We see that the average *ø* value for temperature change from 23C to –150C is 13.87 where as the *ø* value for temperature change from –150C to 23C is only 0.564, which again explain that the microcrack growth is large with reducing temperature and the growth is minimal when taken back to room temperatures. However these values are composite dependent. Although we see a trend of increase of acoustic events with reduction of temperature, the number of events corresponding to a given temperature is not reproducible. For example, the number of events for one sample is as high as 3789 and for another sample is only 1280. This is possibly because during manufacturing process the cure temperatures might be different and at different locations. No tests were done with GFRP composites but it is expected that GFRP samples will also show the similar behavior.

The cracks formed at cryogenic temperatures will remain even after the sample is allowed to attain room temperature. As discussed in the introduction, if the composites are used in reusable space launch vehicles as fuel vessels, the microcracks formed at low temperatures will deteriorate the material and may cause the leakage of the fuel gases. So a good understanding of the permeability of composites is necessary for which an equipment to measure the permeability of composites is conceptually designed and

discussed in previous chapter 4. It is based on the Darcy's law in which the pressure difference across the sample is measured to obtain the permeability value. If the sample is exposed to cryogenic temperatures and has microcracks in it then the pressure in the chamber decreases and the permeability of the sample can be obtained. For more number of microcracks, the pressure decreases at a higher rate and the permeability is high.

6. Conclusions

This chapter summarizes the conclusions drawn from the experimental work performed by shear testing and microcrack monitoring by acoustic emission. It also summarizes the design principles of permeability apparatus.

Interlaminar shear strength increases with decreasing temperatures for both GFRP and CFRP composites. For GFRP composites shear strength increases drastically from 80ºC to 23ºC at the rate of 98psi per ºC and then increase at a low rate of 17.89psi per ºC from 23ºC to –100ºC. For CFRP composites, shear strength increases almost constantly at the rate of 100psi per ºC with decreasing temperatures from 23ºC to –100ºC. It is concluded that polyester matrix in GFRP samples will degrade rapidly with increasing temperatures than epoxy of CFRP samples. The composite materials become more brittle at lower temperatures as seen by sharp peaks for both GFRP and CFRP samples. And as the temperature increases they both become ductile and peaks are flat. It is also observed that GFRP samples are more brittle than CFRP samples at all temperatures as seen by the lower strains at failures. Shear strength of CFRP is more than that of GFRP composites for all temperatures. It is almost double at -100ºC and 50ºC and 1.5 times at -5ºC and 23ºC.

Acoustic emission testing confirmed the microcrack generation in composites at cryogenic temperatures. With the events counted for each microcrack generation, it was observed that during thermal cycling, when the composites are subjected from room to cryogenic temperatures, there are increasing number of microcracks and when the

composite is allowed to attain room temperature back, only very few microcracks are formed.

For a comparative study of microcrack growth with thermal cycling, an index for microcrack growth has been developed as ø, which is defined as the ratio of rate of microcrack growth to the rate of change of temperature. For the CFRP unidirectional (0) 50 ply composites the average value of ø is 13.87 for reducing temperatures from 23ºC to -150ºC and 0.564 for warming temperatures from -150ºC to 23ºC. It shows that once microcrack growth has been completed, the warming phase does not cause any microcrack growth. However these values are composite dependent and as discussed in chapter 5, the number of events corresponding to a particular temperature are not reproducible, which could possibly because during the manufacturing process the cure temperatures were different and at different locations.

To have a good understanding of the microcracks effect on gas permeability of composites, equipment is designed to measure the permeability. The design is based on the Darcy's law that uses the pressure deference across the sample to measure permeability. It has been shown how this apparatus can be used to measure the permeability at room temperatures. And it is also showed how it can be used for measuring permeability of cryogenic temperature gases by immersing it in a low temperature liquid bath (dewar).

References

1. **ASTM**, D 2344-95, (1995), Standard test method for apparent interlaminar shear strength of parallel fiber composites by short-beam method, 1961 Race St., Philadelphia, PA, 19103
2. **Bray D.E. and D. McBride**, (1992), Nondestructive testing techniques, John Wiley and Sons, Inc., NY, pp 8
3. **Broutman L.J. and R.H. Krock,** (1967) Modern composite materials, Addison-Wesley publishing company, Inc., Massachusetts, USA, pp 88
4. **Chawla K.K.**, (1993), Ceramic matrix composites, Chapman and Hall, Cambridge, Great Britain, pp 377, 109
5. **Cogswell F.N.**, (1992), Thermoplastic aromatic polymer composites, Butterworth-Heinemann, Oxford, Great Britain, pp 78, 115, 162, 185, 203, 208
6. **Disder S., J.M. Rey, P. Pailler, A.R. Bunsell,** (1998), "Helium permeation in composite materials for cryogenic application", Cryogenics, Vol. 38, pp 135-142
7. **Dutta P.K. and H.W. Lord**, (1988), "On the design of polymeric composite structures for cold regions applications", Journal of reinforced plastics and composites, Vol. 7, September 1988, pp 436-456
8. **Dutta P.K. and D. Farrell,** (1988), "Acoustic emissions from composites at decreasing temperatures", 6th International congress on experimental mechanics, Vol. 2, SEM, Inc., Portland, pp 1090-1095

9. **Evans D. and R.P. Reed,** (1998), "The permeability of resin based composite materials to radiolytic gases", Cryogenics, Vol. 38, Elsevier science Ltd., pp 149-154
10. **Green W.A. and M. Micunovic**, (1987), Mechanical behavior of composites and laminates, Elsevier science pub. co., Inc., NY, pp 3
11. **Hatta H., Y. Nishiyama, T. Bando, K. Shibuya and Y. Kogo**, (2002), "Gas leakage through C/C composites", 10th US-Japan conference on composite materials, Fu-Kuo Chang, Ed., Sep16-18, Stanford Univ., California, USA, pp 619-626
12. **Hirohata Y., T.Jinushi, Y. Yamauchi, M. Hashiba, T. Hino, Y. Katoh, A. Kohyama**, (2002), "Gas permeability of SiC/SiC composites as fusion reactor material", Fusion engineering and design, Vol. 61-62, pp 699-704
13. **Hollaway L.**, (1993), Polymer composites for civil and structural engineering, Chapman and Hall, Cambridge, Great Britain, pp 57, 126
14. **Hull D.**, (1981), An introduction to composite materials, Cambridge Univ. Press, Cambridge, Great Britain, pp 75, 175-177
15. **Isaac M.D. and O. Ishai**, (1994), Engineering mechanics of composite materials, Oxford univ. press, Inc., NY, pp 26, 265,331
16. **Ishida H.**, (1994), Characterization of composite materials, Butterworth-Heinemann, Boston, pp 53
17. **Jens Humpenoder**, (1998), "Gas permeation of fiber reinforced plastics", Cryogenics, Vol. 38, Elsevier Science Ltd., pp 143-147
18. **Jones R.H.**, (2001), Environmental effects on engineered materials, Marcel Dekker, Inc., NY, pp 429-431

19. **Jones R.M.**, (1975), Mechanics of composite materials, Scripta book company, Washington, preface
20. **Kageyama K.,** (1989), Application of fracture mechanics to composite materials, Friedrich K., Ed., Elsevier, NY, pp 378-381
21. **Kasen M.B.**, (1979), "Cryogenic applications of composite technology", Nonmetallic materials and composites at low temperature, Clark A.K., Reed R.P. and Hartwig G., Ed., Plenum press, NY, pp 326, 333
22. **Kaw A.K.** (1997), Mechanics of composite materials, CRC press, NY, pp 13-14, 155-156
23. **Kim J.K. and Y.W. Mai**, (1998), Engineered interfaces in fiber reinforced composites, Elsevier, Netherlands, pp 46, 240, 329
24. **Lange F.F.**, (1974) Composite materials, Vol. 5, **Broutman L.J., Ed.,** Academic press, NY, pp 21-23
25. **Mallinson J.H.,** (1974) Composite materials, Vol. 3, Noton B.R., Ed., Academic press, NY, pp 360
26. **Mathews F.L. and R.D. Rawlings,** (1994), Composite materials engineering and science, Chapman and Hall, NY, pp 435
27. **Michelove L.D.**, (1979), "Application of graphite-epoxy to cryogenic telescopes", Nonmetallic materials and composites at low temperature, Clark A.K., Reed R.P. and Hartwig G., Ed., Plenum press, NY, pp 404-407
28. **MISTRAS 2001** AEDSP-32/16, Physical Acoustics Corporation, Princeton, NJ

29. **Morse C., O. Ochoa and J. Barron**, (1992), "Permeability and wet-out characterization of srim automotive bumper beams", Composite material technology, Hui D. and Kozik T.J., Ed., ASME, pp 67-69
30. **Motto R.L.,** (1990), applied strength of materials, Prentice hall, NJ, pp 242, 533
31. **Philpot K.A. and R.E. Randolph**, (1982), "The use of graphite/epoxy composites in aerospace structures subject to low temperatures", Nonmetallic materials and composites at low temperature, Hartwig G. and Evans D., Ed., Plenum press, NY, pp 311-325
32. **Pilato L.A. and M.J. Michno,** (1994), Advanced composite materials, Springer-Verlag, Germany, pp 27
33. **Reddy J.N. and A.V. Krishna Murthy**, (1992), Composite structures, Springer-Verlag, NY, pp 198
34. **Schwartz M.M.**, (1992), Composite materials hand book, McGraw-Hill, Inc., NY, pp 7.39
35. **Scott B.R.**, (1959), Cryogenic engineering, Van Nostrand company, Inc., NY, pp 142-213
36. **Sih G.C. and A.M. Skudra**, (1986), Failure mechanisms of composites, Elsevier science pub. Co., Inc., NY, pp 293
37. **Turner F.H.**, (1979), Concrete and cryogenics, Viewpoint publications, NY, pp 79
38. **Weiss W.**, (1982), "Low temperature properties of carbon fiber reinforced epoxide resins", Nonmetallic materials and composites at low temperature, Hartwig G. and Evans D., Ed., Plenum press, NY, pp 293-309

39. **Whitcomb J.,** (2002), "Prediction of microcracking induced permeability of cryogenic composite tanks", NCAM Project No. 58404-S7

40. **Yokozeki T., T. Aoki and T. Ishikawa**, (2002), "Evaluation of gas permeability through CFRP laminates with matrix cracks", 10th US-Japan conference on composite materials, Fu-Kuo Chang, Ed., Sep16-18, Stanford Univ., California, USA, pp 609-618

Bibliography

1. **Adams D.S., D.E. Bowles and C.T. Herakovich**, (1986), "Thermally induced transverse cracking in graphite/epoxy cross-ply laminates", Journal of reinforced plastics and composites, Vol. 5, pp 152-169
2. **Aoki T., T. Ishikawa, H. Kumazawa and Y. Morino**, (2000), "Mechanical performance of CF/Polymer composite laminates under cryogenic conditions", AIAA conference paper, 2000-1605
3. **ASTM**, D 2344-95, (1995), Standard test method for apparent interlaminar shear strength of parallel fiber composites by short-beam method, 1961 Race St., Philadelphia, PA, 19103
4. **Barnes J.A. and F.N. Cogswell**, (1989), "Thermoplastics for space", SAMPE Quarterly, Vol. 20(3), pp 22-27
5. **Bascom W.D.**, (1965), "Some surface chemical aspects of glass-resin composites and wetting behavior of epoxy resins on glass filaments", 20th conference SPI reinforced plastics division, Section 15-B
6. **Berthelot J.M. and J. Billand**, (1983), 1st International symposium on AE from reinforced composites, Society of plastics industry, California, USA
7. **Bowles D.A.**, (1984), "Effect of microcracks on the thermal expansion of composite laminates", Journal of composite materials, Vol. 17, pp 73-187

8. **Bray D.E. and D. McBride**, (1992), Nondestructive testing techniques, John Wiley and Sons, Inc., NY, pp 8
9. **Broutman L.J. and R.H. Krock,** (1967) Modern composite materials, Addison-Wesley publishing company, Inc., Massachusetts, USA, pp 88
10. **Camahort J.L., E.H. Rennhack and W.C. Coons**, (1976), "Effects of thermal cycling environment on graphite/epoxy composites", Environmental effects on advanced composite materials, ASTM STP 602, American society of testing and materials, pp 37-49
11. **Chawla K.K.**, (1993), Ceramic matrix composites, Chapman and Hall, Cambridge, Great Britain, pp 377, 109
12. **Cogswell F.N.**, (1987), "The processing science of thermoplastic structural composites", International polymer processing, Vol. 1(4), pp 157-165
13. **Cogswell F.N.**, (1992), Thermoplastic aromatic polymer composites, Butterworth-Heinemann, Oxford, Great Britain, pp 78, 115, 162, 185, 203, 208
14. **Cohen D., M.W. Hyer and S.S Tomkins**, (1984), "Effects of thermal cycling on matrix cracking and stiffness changes in composite tubes", 16th National SAMPE technical conference, pp 577-588
15. **Cohen L.J. and O. Ishai**, (1967), Journal of composite materials Vol. 1, pp 390
16. **Daniel I.M. and T. Liber**, (1975), Lamination residual stresses in fiber composites, Interim report NASA CR-134826, IITRI D6073-I
17. **Dave R., J.L. Kardos and M.P. Dudukovic**, (1987), "A model for resin flow during composite processing: Part1- General mathematical development", Polymer composites, Vol. 8(1), pp 29-38

18. **Disder S., J.M. Rey, P. Pailler, A.R. Bunsell,** (1998), "Helium permeation in composite materials for cryogenic application", Cryogenics, Vol. 38, pp 135-142
19. **Dutta P.K. and H.W. Lord**, (1988), "On the design of polymeric composite structures for cold regions applications", Journal of reinforced plastics and composites, Vol. 7, September 1988, pp 436-456
20. **Dutta P.K. and D. Farrell,** (1988), "Acoustic emissions from composites at decreasing temperatures", 6th International congress on experimental mechanics, Vol. 2, SEM, Inc., Portland, pp 1090-1095
21. **Eselun S.A., H.D. Neubert and E.G. Woff**, (1979), "Microcracking effects on dimensional stability", Society of advanced material and process engineering (SAMPE), Vol. 24(2), pp 1299-1309
22. **Evans D. and J.T. Morgan**, (1984), "Cryogenic containment in composite vessels", Advanced cryogenic engineering materials, Vol. 34, pp 11
23. **Evans D. and R.P. Reed,** (1998), "The permeability of resin based composite materials to radiolytic gases", Cryogenics, Vol. 38, Elsevier science Ltd., pp 149-154
24. **Evans D., S.J. Robertson, S. Walmsley and J. Wilson**, (1988), "Measurement of the permeability of carbon/peek composites", Cryogenic materials, Vol. 2, Structural materials, pp 755-763
25. **Evans D., S.J. Robertson, S. Walmsley and J. Wilson**, (1989), "Measurement of the permeability of carbon/peek composites", Rutterford Appleton laboratory
26. **Fahmy A. and T.G. Cunningham**, (1976), "Investigation of thermal fatigue in fiber composite materials", Final report, NASA CR-2641

27. **Fowler T.J.**, (1977), "AE of fiber reinforced plastics", ASCE fall convention and exhibit, preprint 3092, October

28. **Fowler T.J. and E. Gray**, (1979), "Development of an AE test for FRP equipment", ASCE convention and exposition, preprint 3583, Boston

29. **Funk J.G. and G.F. Sykes**, (1988), "Space radiation effects on poly thin films and composites", SAMPE Quarterly, Vol. 19(3), pp 19-26

30. **Givler R.C, J.W. Gillespie, Jr. and R.B. Pipes**, (1982), " Environmental exposure of carbon/epoxy composite material systems", Composites for extreme environments, ASTM STP 768, American society for testing and materials, pp 137-147

31. **Green W.A. and M. Micunovic**, (1987), Mechanical behavior of composites and laminates, Elsevier science pub. co., Inc., NY, pp 3

32. **Guild F.J., M.G. Phillips and B. Harris**, (1980), "AE studies of failure in GRP", NDT International, Vol. 13, pp 209-218

33. **Gutowski T.G.**, (1985), "A resin flow/fiber deformation model for composites", SAMPE Quarterly, Vol.16, pp 58-64

34. **Gutowski T.G., Z. Cai, J. Kingery and S.J. Williams**, (1986), "Resin flow/fiber deformation experiments", SAMPE Quarterly, Vol. 17(4), pp 54-58

35. **Hatta H., Y. Nishiyama, T. Bando, K. Shibuya and Y. Kogo**, (2002), "Gas leakage through C/C composites", 10th US-Japan conference on composite materials, Fu-Kuo Chang, Ed., Sep16-18, Stanford Univ., California, USA, pp 619-626

36. **Hirohata Y., T.Jinushi, Y. Yamauchi, M. Hashiba, T. Hino, Y. Katoh, A. Kohyama**, (2002), "Gas permeability of SiC/SiC composites as fusion reactor material", Fusion engineering and design, Vol. 61-62, pp 699-704

37. **Hollaway L.**, (1993), Polymer composites for civil and structural engineering, Chapman and Hall, Cambridge, Great Britain, pp 57, 126

38. **Hull D.**, (1981), An introduction to composite materials, Cambridge Univ. Press, Cambridge, Great Britain, pp 75, 175-177

39. **Hyer M.W.**, (1986), "Thermal stresses in composite tubes", International symposium on composite materials and structures, Beijing, pp 246-251

40. **Hyer M.W., D.W. Cooper and D. Cohen**, (1986), "Stresses and deformations in cross-ply composite tubes subjected to a uniform temperature change", Journal of thermal stresses, Vol. 9, pp 97-117

41. **Isaac M.D. and O. Ishai**, (1994), Engineering mechanics of composite materials, Oxford univ. press, Inc., NY, pp 26, 265,331

42. **Ishida H.**, (1994), Characterization of composite materials, Butterworth-Heinemann, Boston, pp 53

43. **Jens Humpenoder**, (1998), "Gas permeation of fiber reinforced plastics", Cryogenics, Vol. 38, Elsevier Science Ltd., pp 143-147

44. **Jones R.H.**, (2001), Environmental effects on engineered materials, Marcel Dekker, Inc., NY, pp 429-431

45. **Jones R.M.**, (1975), Mechanics of composite materials, Scripta book company, Washington, preface

46. **Judd N.C.W. and W.W. Wright**, (1978), "Voids and their effects on the mechanical properties of composites" – an appraisal, SAMPE Journal, Jan./Feb., pp 10-14

47. **Kageyama K.,** (1989), Application of fracture mechanics to composite materials, Friedrich K., Ed., Elsevier, NY, pp 378-381

48. **Kasen M.B.**, (1979), "Cryogenic applications of composite technology", Nonmetallic materials and composites at low temperature, Clark A.K., Reed R.P. and Hartwig G., Ed., Plenum press, NY, pp 326, 333

49. **Kaw A.K.** (1997), Mechanics of composite materials, CRC press, NY, pp 13-14, 155-156

50. **Kim J.K. and Y.W. Mai**, (1998), Engineered interfaces in fiber reinforced composites, Elsevier, Netherlands, pp 46, 240, 329

51. **Kumazawa H., T. Aoki, T. Ishikawa and I. Susuki**, (2001), "Modeling of propellant leakage through matrix cracks in composite laminates", AIAA conference paper, pp 2001-1217

52. **Lam R.C. and J.L. Kardos**, (1988), "The permeability of aligned and cross-plied fiber beds during processing of continuous fiber composites", American society of composites, 3rd Annual technical conference, pp 3-11

53. **Lange F.F.**, (1974) Composite materials, Vol. 5, **Broutman L.J., Ed.,** Academic press, NY, pp 21-23

54. **Lundemo C.Y. and S.E. Thor**, (1977), "Influences of environmental exposure of carbon/epoxy composite materials", Journal of composite materials, Vol. 11, pp 276-284

55. **Mallinson J.H.,** (1974) Composite materials, Vol. 3, Noton B.R., Ed., Academic press, NY, pp 360

56. **Mathews F.L. and R.D. Rawlings,** (1994), Composite materials engineering and science, Chapman and Hall, NY, pp 435

57. **Mazzio V.F., R.L. Mehan and J.V. Mullin,** (1973), "Basic failure mechanisms in advanced composites", NASA-CR-134525, NASA-Lewis research center, Contract NAS3-15835

58. **Mehan R.L. and J.V. Mullin**, (1971), "Analysis of composite failure mechanisms using AE", Journal of composite materials, Vol. 5, pp 266-269

59. **Michelove L.D.**, (1979), "Application of graphite-epoxy to cryogenic telescopes", Nonmetallic materials and composites at low temperature, Clark A.K., Reed R.P. and Hartwig G., Ed., Plenum press, NY, pp 404-407

60. **MISTRAS 2001** AEDSP-32/16, Physical Acoustics Corporation, Princeton, NJ

61. **Morse C., O. Ochoa and J. Barron**, (1992), "Permeability and wet-out characterization of srim automotive bumper beams", Composite material technology, Hui D. and Kozik T.J., Ed., ASME, pp 67-69

62. **Motto R.L.,** (1990), applied strength of materials, Prentice hall, NJ, pp 242, 533

63. **Nishijima S. and T. Okada, K. Fujioka, Y. Kuraoka**, (1988), "Gas permeation and performance of an FRP cryostat", Cryogenics, Vol. 28(4), pp 285

64. **Paul J.T., Jr. and J.B. Thomson**, (1965), "The importance of voids in the filament wound structure", 20th Conference of SPI reinforced plastic division, Section 12-C

65. **Philpot K.A. and R.E. Randolph**, (1982), "The use of graphite/epoxy composites in aerospace structures subject to low temperatures", Nonmetallic materials and composites at low temperature, Hartwig G. and Evans D., Ed., Plenum press, NY, pp 311-325

66. **Pilato L.A. and M.J. Michno,** (1994), Advanced composite materials, Springer-Verlag, Germany, pp 27

67. **Reddy J.N. and A.V. Krishna Murthy**, (1992), Composite structures, Springer-Verlag, NY, pp 198

68. **Rey J.M., B. Gallet, J.M. Baze and A.R. Bunsell**, (1992), "Helium diffusion and mechanical properties of glass fiber reinforced epoxy at cryogenic temperature", Composite polymers, Vol. 5(3), pp 205

69. **Rossi R.C.**, (1969), Journal of American ceramics society, Vol. 52, pp 290

70. **Rotem A.**, (1977), "The discrimination of micro-fracture modes of fibrous composite materials by AE technique". Fiber science technology, Vol. 10, pp 101-120

71. **Schwartz M.M.**, (1992), Composite materials hand book, McGraw-Hill, Inc., NY, pp 7.39

72. **Scott B.R.**, (1959), Cryogenic engineering, Van Nostrand company, Inc., NY, pp 142-213

73. **Sih G.C. and A.M. Skudra**, (1986), Failure mechanisms of composites, Elsevier science pub. Co., Inc., NY, pp 293

74. **Sims G.D.**, (1976), "Stress wave emission from polymeric materials, plastic, rubber", Material Applications, Vol. 2, pp 205-215

75. **Speake J.H. and C.J. Curtis**, (1974), "Characterization of fracture processes in CFRP using spectral analysis of AE arising from the application of stress", International conference on carbon fibers, their place in modern technology, London, Paper No. 29

76. **Sullivan L.J. and R. Ghaffarian**, (1988), SAMPE 33, pp 1604

77. **Sundaresan M.J., E.G. Henneke and A. Gavens**, (1989), "NDE procedure for predicting the fatigue life of composite structural members", World meeting on AE, Charlotte, NC, March 20-23

78. **Sykes G.F., J.G. Funk and W.S. Slemp**, (1986), "Assessment of space environment induced microdamage in toughened composite materials", 18th International SAMPE technical conference

79. **Tompkins S., G.F. Sykes and D.E. Bowles**, (1985), "The thermal and mechanical stability of composite materials in space structures", Soc. Mfg. Eng. space technical conference, Anaheim, California, Paper No. EM85-979

80. **Turner F.H.**, (1979), Concrete and cryogenics, Viewpoint publications, NY, pp 79

81. **Weiss W.**, (1982), "Low temperature properties of carbon fiber reinforced epoxide resins", Nonmetallic materials and composites at low temperature, Hartwig G. and Evans D., Ed., Plenum press, NY, pp 293-309

82. **Wheeler A.J.**, (1990), PhD thesis, University college of Wales, Aberystwyth

83. **Will E.T.**, (1994), "Screening program to select a resin for gravity probe composites", Cryogenics, Vol. 32(2), pp 179

84. **Williams J.G., C.E.M. Morris and B.C. Ennis**, (1974), "Liquid flow through aligned fiber beds", Polymer engineering and science, Vol. 14(6), pp 413-419

85. **Williams R.S. and K.L. Reifsnider**, (1974), Journal of composite materials, Vol. 8, pp 340

86. **Whitcomb J.,** (2002), "Prediction of microcracking induced permeability of cryogenic composite tanks", NCAM Project No. 58404-S7

87. **Yokozeki T., T. Aoki and T. Ishikawa**, (2002), "Evaluation of gas permeability through CFRP laminates with matrix cracks", 10th US-Japan conference on composite materials, Fu-Kuo Chang, Ed., Sep16-18, Stanford Univ., California, USA, pp 609-618

Vita

The author received her Bachelor of Technology degree from Jawaharlal Nehru Technological University, India in July 2001. The author came to United States of America in August 2001 for further studies. She is now completing her Master of Science degree in Mechanical Engineering at the University of New Orleans, New Orleans, LA.